~~Universal~~ Traveling-wave antenna model for terahertz radiation from laser-plasma interactions

Jiayu Zhao,[1,2] Yuchen Hui,[1] Yamin Chen,[1] Zuanming Jin,[1] Alexander P. Shkurinov,[3] Yan Peng,[1,2,4] Yiming Zhu[1,2,*] and Songlin Zhuang[1]

[1] Terahertz Technology Innovation Research Institute, Shanghai Key Laboratory of Modern Optical Systems, School of Optical-Electrical and Computer Engineering, University of Shanghai for Science and Technology, Shanghai 200093, China.
[2] Shanghai Institute of Intelligent Science and Technology, Tongji University, Shanghai 200092, China.
[3] Faculty of Physics and International Laser Center, Lomonosov Moscow State University, Moscow 119991, Russia.
[4] py@usst.edu.cn
* ymzhu@usst.edu.cn

Abstract

Generation of terahertz (THz) wave from air plasma induced by femtosecond laser pulses with a single central frequency (the so-called "single-color") is one of the fundamental interactions between light and matter, and is also the basis of subsequent pumping schemes using two- or multi-color laser fields. Recently, more states of media beyond gas (e.g., atomic cluster and liquid) via photo-ionization have brought new experimental observations of THz radiation, which can no longer be simply attributed to the mainstream model of the transition-Cherenkov radiation (TCR), thus making the whole picture unclear. Here, we revisited the mechanism of this dynamic process in a new view of the traveling-wave antenna (TWA) model. By successfully reproducing the reported far-field THz radiation profiles from various plasma filament arrangements, the ~~universal~~ wide applicability of the TWA theory has been revealed. On the other hand in the microscopic view, we investigated the plasma oscillation during filamentation aiming at further bridging the plasma filament and the antenna. Accordingly, THz-plasma resonance has been theoretically and experimentally demonstrated as the elementary THz emitter, paving the way towards fully understanding this important single-color plasma based THz source.

Keywords: Traveling-wave antenna, Plasma filament, Cherenkov radiation, THz generation, Physical mechanism

1. INTRODUCTION

The well-known Cherenkov radiation [1,2] describes notable properties of radiation which appears during the motion of electrically charged particles through a substance with a velocity exceeding that of light in the same medium. In practice, the speed of the energetic charge doesn't have to be considerably superluminal since its moving trajectory normally has a finite length [3]. In this situation, boundary effects of the length-limited path also contribute to the observed radiation (i.e., the particle is assumed to gain accelerated velocities at both ending points of the trajectory) [4], and thus the Cherenkov radiation holds some features of the transition radiation [4,5] or bremsstrahlung radiation [4]. For the above reasons, the concept of transition-Cherenkov radiation (TCR) was proposed by authors of Ref. [6,7] to describe the terahertz (THz) emission from dipole-like charges moving behind the laser ionization front (at the velocity of c [6]) during single-color femtosecond laser filamentation process. Finally, the TCR theory turns into the modern view for interpreting the underlying mechanism of THz wave generation from a single-color filament [8-13], which is another milestone ever since the first demonstration in 1993 [14] of this fundamental interaction between light (intense laser) and matter (air).

However, the literal meaning of "transition-Cherenkov" is likely misleading, which cannot be understood as a real mixture of the two physical processes [15,16], since no "transition" of particles at boundaries between two media was actually involved in Ref. [6,7]. On the other hand, as for "Cherenkov", there is in fact few strong evidence for the speed of pumping laser dramatically exceeding that of the radiated THz wave, and this superluminality of the laser propagation has also been clarified to be not strictly necessary [3]. Furthermore, the recent hot topic of laser-induced plasma inside a liquid medium for THz wave generation [17], and the backward THz radiation featured interactions between laser and gas cluster [18], have started to fall out of scope of the TCR mechanism. Thus a more applicable theoretical frame remains as the challenge.

Remind ourselves that the TCR model is not the only option in order to account for the characteristic conical forward THz emission from a single-color filament. Meanwhile in the microwave community, another classical model of traveling-wave antenna (TWA) [19,20] can also give birth to THz conical radiations in many flexible patterns. More importantly, the TWA model shares similar properties with the TCR theory, that is the moving point source (in TWA case, it is the current element) with a finite propagation path (in TWA case, it is the antenna itself) and accelerated velocities at both boundaries of the path [21]. Moreover, the TWA model presents its three building blocks (i.e., the element, array and space factors) in quite a concise manner as can be

seen in Table I-IV, thus offering a new picture for understanding the THz wave generation from laser filaments. It is also worth mentioning that, we are delighted to see a similar thought with this work in a very recent publication [22], which has also treated the laser filaments as pulsed antennas for interpreting the THz-microwave radiation. Hence, this novel antenna's point of view is just being unfolded with many follow-up works to be deeply explored.

In the current paper, the TWA model was re-worked and improved to analytically investigate the emission properties of THz wave during single-color filamentation. Briefly, in the following Section 2, far-field profiles of THz radiation from different plasma sources were studied via the TWA method, such as a single filament without or with a longitudinal/transverse static electric field, double filaments in Vee or parallel arrangement, a micro-filament induced by laser-atomic cluster interaction, and a micro-filament excited in the water film. We have demonstrated good agreements between our theoretical results and a number of experimental observations from previous publications [6,8-12,17,18]. While in Section 3, the TWA model was extended in a microscopic point of view. In short, the plasma electron oscillations during filamentation were illustrated to play the role of current elements of the TWA model, and the resonance radiation of plasma oscillators was revealed to account for THz wave generation. At last, this resonance effect has been verified by experimentally exploring its accompanying phenomenon, which is the temporal advance of THz waveforms in a bandwidth-limited detection system.

It is worth noting that, with plenty of experimental facts in Table I-IV (including distinctly different photo-ionization media and THz radiation profiles) unified in the ~~universal~~ framework of the TWA theory, we may contribute to the recent tendency of unifying different mechanisms in a specific filamentation process. For our work, it is totally associated with the single-color laser pumping THz wave generation scheme. In other situations, e.g., in field of two-color laser excitation, four-wave mixing (4WM) and transient photocurrent (PC) models were successfully combined by building their intrinsic connections during photo-ionization of air [23-25]. Recently, a unified model was even reported [26] for both one- and two-color laser induced THz waves from a liquid, which are believed to be based on completely different mechanisms and have usually been considered separately in the previous literature. These works offer new ideas to the community for better interpreting the THz physics in a complex laser filamentation phenomenon.

2. FAR-FIELD THZ RADIATION PROFILES FROM DIFFERENT TWA-LIKE PLASMA FILAMENT ARRANGEMENTS

Linear antennas, whose current distributions can be represented by traveling waves in the same direction, are referred to as traveling-wave antennas (TWA). And the corresponding TWA model describes electromagnetic (EM) radiations from this antenna, which can be written as [19,22,27]

$$E(\omega,\theta,l) = \frac{\eta}{2\pi r} \cdot j_0(\omega)\sin\theta \cdot Q(\omega,\theta,l) \qquad (1)$$

where η is the intrinsic impedance, r and θ are for the polar coordinates with θ defined as the angle relative to the current axis (z), $j_0(\omega)$ is the spectral current, and l is the antenna length. As mentioned in the Introduction, the TWA model presents its formulas with three building blocks, namely, the element, array and space factors. In view of Eq. (1), the element factor (current element) is written as $j_0(\omega)\sin\theta$, which indicates the type of current and its direction of flow. In case of different plasma filament configurations, this element factor changes which can be seen in Table I-IV. As for the array factor, it will be introduced when the filaments array is studied in Section 2.5. And the space factor is $Q(\omega,\theta,l)$, which provides an accurate description of the phase matching condition as discussed below.

In case of THz wave emissions from a plasma-filament-based antenna, $Q(\omega,\theta,l) = \sin[(kl/2)(K-\cos\theta)]/(K-\cos\theta)$ with $k = \omega/c$ and $K = v_{THz}/v_{g,laser}$ where $v_{THz} = c/n_{THz}$ is the THz phase velocity at ω, and $v_{g,laser} = c/n_{g,laser}$ is the group velocity of the driven laser, as well as the speed of the ionization front and the traveling-wave current [22]. Normally, K ($= n_{g,laser}/n_{THz}$) ≤ 1 needs to be fulfilled in order to achieve the Cherenkov-type phase matching between the traveling-wave current (also the pumping laser pulse) and the field that this current radiates [22]. However, the superluminality of the laser propagation is not strictly necessary, as in the Sprangle model [3], and the THz source is generated even if the velocity of the laser ionization front is exactly the light velocity [6, 7], because the THz wave can be produced due to the very finite length of the filament ($l\sim$10 mm) [7]. Thus for convenience of the following calculations, $n_{g,laser} \approx n_{THz}$ is considered, i.e., K is set as 1. Hence the final expression of the radiated θ-dependent distribution at a certain ω is

$$|E(\omega, \theta, l)| \propto |\sin\theta| \cdot \left| \frac{\sin[(kl/2)(1-\cos\theta)]}{1-\cos\theta} \right|$$

(2)

In this case, radiations in the forward direction, i.e., along the z axis, are strongly suppressed by the $|\sin\theta|$ factor [22], which leads to the typical off-axis conical THz profile, as can be seen in Table I-IV.

2.1 A single filament

The element and space factors of a single filament are listed in the top row of Table I. In the same row, the schematic of a current element is also shown (as the horizontal double-headed arrow) whose oscillation direction is parallel to the z axis of the filament (as the dashed line), together with its radiation profile ("8"-shaped curves) involving off-axis maximums given by $|\sin\theta|$.

Corresponding calculations were carried out at 0.1 THz for three filament lengths of l = 10, 30 and 100 mm. One can see that the resulted THz emission is typically in a conical shape due to the on-axis non-radiation characteristic of current elements $|\sin\theta|$. Moreover, a larger cone angle is obtained in case of a shorter filament, which can be well verified by the experimental patterns in Table I adapted from Ref. [6]. If the filament length is further decreased to a sub-millimeter size, the radiation pattern of the filament will be approximately like that of a current element in "8" shape. This is exactly what can be found in Ref. [28] that the THz radiation direction was nearly orthogonal to the z axis. Next, we improved the TWA model and examined it in more different situations.

2.2 A filament with a longitudinal DC field

When the plasma filament is applied with an external DC electric field in the longitudinal direction, i.e., E_{ex}^l of the order of magnitude of kV/cm or larger, the oscillation of current element will be greatly intensified (details in the Supplemental Material A-B). Thus a coefficient $n = 1 + |E_{ex}^l/E_w|$ is introduced to quantitatively characterize this enhancement, as shown in the second row of Table I, where $E_w \sim 0.2$ kV/cm [7] is the laser wakefield amplitude.

Then, the 0.1 THz radiation pattern produced from a 10-mm-length filament has been calculated with $E_{ex}^l = 0$, 5 and 10 kV/cm, as black, blue and red lines, respectively. For comparison purposes, the three patterns are normalized to that of $E_{ex}^l = 10$ kV/cm. Compared with the experimental results in the same row from Ref. [8], one can observe the same phenomenon that the radiated THz intensity is increased by the longitudinal electric field, while its angular distribution remains the same.

2.3 A filament with a transverse DC field

THz wave radiation from a plasma filament under transverse electric fields E_{ex}^t is also taken into account. This time, the THz driven current is additionally combined with a transverse current besides the original longitudinal one (details in the Supplemental Material C). A quantitative description of this effect via the TWA theory can be that the direction of the current element is rotated by a certain angle $\varphi = \arctan(E_{ex}^t/E_w)$ as shown in the third row of Table I. In this condition, the symmetry of the 0.1 THz radiation pattern from a filament (l = 20 mm) is broken. With a larger bias voltage (i.e., a larger φ), the convergence of two lobes develops towards the z axis and keeps asymmetrical all the time. This external field effect has also been observed in Ref. [9] as shown as the experimental results in the same row.

When the bias voltage reaches saturation values making φ into 90°, the current element will oscillate perpendicularly to the z axis, as shown in the fourth row. Under this circumstance, the produced 0.1 THz radiation after the laser filament (l = 15, 50 and 100 mm) is on-axis restrained in a smaller angular distribution for a longer filament. This well agrees with the experimental results in Ref. [9].

2.4 Vee bi-filaments

In this section, we studied the THz radiation from a Vee-antenna constituted by dual-filaments with a crossed half angle α, as shown in the Row 1 of Table II. Here, θ in $E(\omega,\theta,l)$ is replaced by $(\theta+\alpha)$ for the upper filament, or by $(\theta-\alpha)$ for the lower one. Then, two situations are considered: THz waves from the two filaments are (i) in phase and expressed as $|E(\omega,(\theta+\alpha),l)+E(\omega,(\theta-\alpha),l)|$; (ii) out of phase as $|E(\omega,(\theta+\alpha),l)-E(\omega,(\theta-\alpha),l)|$. Meanwhile, α and l were set to be 32° and 10 mm, respectively.

The calculation outcomes for emission profiles at 0.1 THz from this V-shaped filaments array are displayed in Row 1 of Table II. For case (i), THz waves from the two filaments achieve destructive interference and cancellation in the z direction. While for case (ii), the THz intensity is enhanced by ~4 times along the z axis due

to constructive interferences. These two patterns well match the experimental results in Ref. [10] as shown in the right side of the same row. It is worth mentioning that, our results are even closer to these experimental observations than the theoretical results in Ref. [10] given by the TCR model.

2.5 Parallel bi-filaments

In another condition of a plasma array being formed by two parallel filaments, the entire THz wave emission is the superimposition of THz radiations from parallel-oscillated current elements along both filaments (in Table II). In our model, the array factor $|\cos(kd\sin\theta/2-\beta/2)|$ is introduced, where d and β denote the spatial separation and relative temporal (phase) delay between two parallel filaments, respectively. Now, the total THz radiation of the bi-filaments is the product of element, array and space factors.

We first varied d (= 0.5, 2.4 and 3.4 mm) with a fixed β (= 0) and studied the synthesized 0.1 THz intensity profile from 10-mm-long bi-filaments. The corresponding three calculation results are shown in the second row of Table II. It can be seen that with the increasing of d, the THz radiation diminishes but remains symmetric. Similar experimental phenomena were also observed in Ref. [11].

Next, we considered different β (0-2π) between THz pulses from the laser filaments with a fixed d at 2.4 mm. This time, the THz radiation pattern undergoes asymmetrical changes as recorded in the third to fifth rows of Table II. Briefly, to begin with $\beta = 0$, the THz emission is symmetric. With the growth of β, the radiation pattern becomes asymmetric. When β equals $\pi/4$ or $7\pi/4$, the THz angular profile is completely in the direction of one single lobe. With further delay (after $\beta = \pi$), the other lobe starts to rise at the sacrifice of the former. At $\beta = 2\pi$, the radiated THz pattern is identical to the one without time/phase delay (i.e., the first figure in Row 3). Finally, good agreements between our calculations and experimental reports in Ref. [11] can be clearly seen in Table II.

2.6 Parallel bi-filaments with a transverse DC field

In Table III, on the basis of the above parallel bi-filaments, an additional transverse DC field was applied. In this case, the element factor $|\sin\theta|$ has been turned into $|\cos\theta|$ according to the last row of Table I. Meanwhile, the other factors are unchanged. Afterwards, the same calculation processes as the ordinary parallel bi-filaments (in Table II) have been repeated and the results are presented in the top four rows of Table III. In Row 1, for a larger distance d between two filaments ($\beta = 0$), the THz emission pattern becomes less opening, but remains to be symmetrical around the z axis. In Row 2-4, for a varied β (0-2π) and a fixed d (2 mm) between the double filaments, the resulted THz emission pattern gradually turns to be asymmetrical, alternatively oriented to one side of the z axis. These characteristic evolutions of THz far-field profiles have been well reproduced in reported experiments [12].

2.7 A filament with transverse jet of atomic cluster

In this section, the THz radiation from atomic cluster plasma was investigated. As for this scheme, electrons in the plasma column are partly driven away from the laser propagation direction, which accordingly generates a transverse current element, preferring to be parallel to the direction of gas injection [18]. Combined with the original current element along the z axis, a quasi-quadrupole is created for the element factor which can be described as $|\sin\theta \times\cos\theta|$. A typical angular distribution of THz radiation from this orthogonal current element inside the plasma cluster was calculated at 0.1 THz and shown in Row 5 of Table III, in which it can be seen that four lobes are in about ±45° with respect to the laser propagation axis.

When the filament length l is increased from 0.7 to 1.8 mm, the whole THz emission pattern keeps symmetrical and the backward lobes gradually fade away. This property of backward THz emission from a short plasma filament induced by laser-cluster interaction has also been experimentally confirmed in Ref. [18] as shown in the same row. The remaining discrepancy of the angle of main lobes between our calculated patterns (±45°) and the reported observation (±30°) might be attributed to the fact that, a broadband THz signal was measured by the used bolometer in the literature [18], while our results were calculated at a single THz frequency. Moreover, this backward THz emission phenomenon cannot be easily explained by the popular Cherenkov-type mechanism.

2.8 A filament excited in the water film

In recent years, great efforts have been made on new states of matter (beyond gas and solid) being photo-ionized for THz wave generation, such as liquid THz sources. Water films [17,29-37] in both flowing and static forms were studied, as well as the liquid nitrogen [38,39] or even the liquid metal [40,41]. The generated THz energy was proved to be >10 times larger than that achieved from the most standard table-top technique, i.e., the two-color filament in air [37]. Here in this section, we show that this new liquid-plasma target, inside which THz wave radiates, also follows the basic nature of the improved TWA theory.

Taking a water film as an example which is drawn in light blue color in Table IV, the incident laser beam produces two angles of α and θ_r when it is refracted on the interface between air and water. Inside the water film, a micrometer-length filament is created at the laser focus and radiates THz wave, which then makes angles of θ_t and $|\beta-\alpha|$ during propagation through the other water-air interface towards the detection point (marked with an eye). Here, $|\beta-\alpha|$ denotes the detection direction with respect to the horizontal z axis, where β is the included angle between directions of the detection and the initial laser propagation. Note that, the minus (-) is written due to the opposite signs between β and α. Furthermore, $\theta_r = \arcsin[\sin(-\alpha)/n_{laser}]$ and $\theta_t = \arcsin[\sin(\beta-\alpha)/n_{THz}]$ according to the Snell's Law applied on both surfaces of the water film. $n_{THz} = 2.33$ and $n_{laser} = 1.33$ [42] are the refractive indices of THz wave and laser inside the water, respectively.

As for the above filament, its THz emission pattern can be easily described by replacing θ in $E(\omega,\theta,l)$ with ($\theta_t + \theta_r$). At the same time, the laser energy loss caused by its reflection on the air-water interface is also taken into account by introducing the attenuation factor of $(1-r^2)$, where r follows the Fresnel Equation expressed as $r = (\cos\alpha-n_{laser}\times\cos\theta_r)/(\cos\alpha+n_{laser}\times\cos\theta_r)$. On the other hand, however, the THz energy loss due to the water absorption is not considered for the following reasons. According to Ref. [17], the THz intensity through the water film is given by $I_{THz} = I_0\exp[-\alpha'd/(2\cos\theta_t)]$, where $\alpha' = 100$ cm^{-1} is the power absorption coefficient, and $d = 120$ μm is the thickness of the water film. On the water-to-air interface, THz waves can't be coupled out if its total internal reflection occurs, and the critical angle can be easily calculated as 25 degree. Thus θ_t varies between -25 and +25 degree, and I_{THz} is between $0.51I_0$ and $0.54I_0$, where $\Delta = 0.03I_0$ is negligible when profiling the angular distribution of the THz radiation. At last, calculations for the THz wave generation (centered at $f = 0.5$ THz) from a micro-plasma filament ($l = 40$ μm) were performed by multiplying the two factors of element and space in Table IV with the attenuation factor.

The resultant THz intensities I_{THz} are plotted as a function of α in Table IV (as red lines) with β fixed at 0° or 55°, providing good reproductions of the reported results in experiments [17]. On the other hand, $I_{THz}(\alpha,\beta)$ was also calculated and shown in Table IV as the 2-D figure. Compared with the reported one on the right-hand side, the overall trends of I_{THz} evolution along α and β are exactly the same. That is, with the increase of β, the I_{THz} dip gradually shifts towards a greater α. Note that contradictions appear near the white dashed lines (given by $|\beta-\alpha| = 90°$) in the two figures, where I_{THz} achieved minimum in the publication. This point is easily understood since I_{THz} cannot be observed in the direction orthogonal to the horizontal z axis (i.e., $|\beta-\alpha| = 90°$), where the water film either blocks the detector or seriously reduces the THz energy. For the sake of convenience, this issue is neglectable in our model.
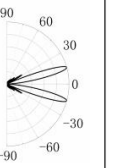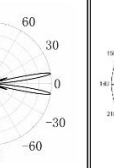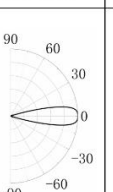
Table I.
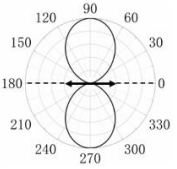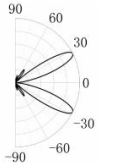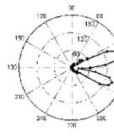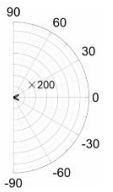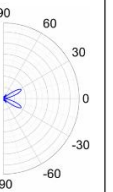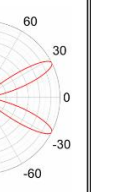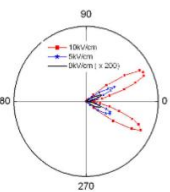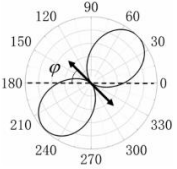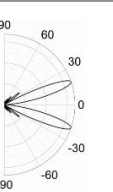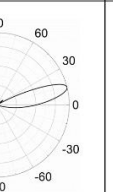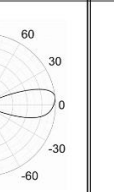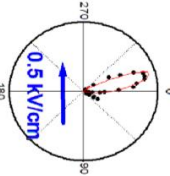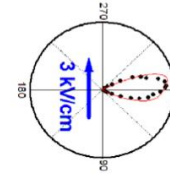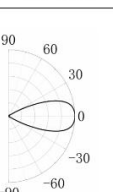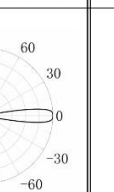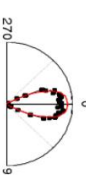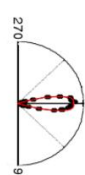
The re-worked traveling-wave antenna (TWA) model			Our calculations				Reported experiments			
Type	Element factor	Space factor	Current element	$l=10$ mm	30 mm	100 mm	~10 mm	~30 mm	80 mm	
Single filament	$\|\sin\theta\|$	$\left\|\dfrac{\sin[\dfrac{kl}{2}(1-\cos\theta)]}{1-\cos\theta}\right\|$								[6]
Single filament with a longitudi-nal DC field	$n\|\sin\theta\|$			0 kV/cm	5 kV/cm	10 kV/cm	0 (black), 5 (blue) and 10 (red) kV/cm			[8]
Single filament with a transverse DC field	$\|\sin(\theta+\varphi)\|$ or $\|\cos\theta\|(\varphi=90°)$			0 kV/cm	0.1 kV/cm	1 kV/cm	0.5 kV	3 kV		[9]
				$l=15$ mm	50 mm	100 mm	15 mm	50 mm		

Table II.
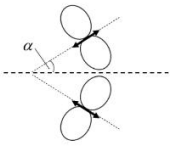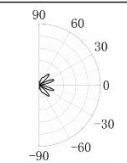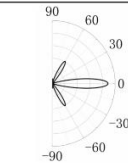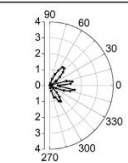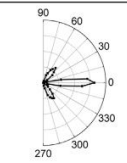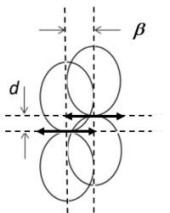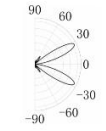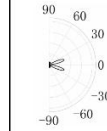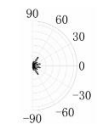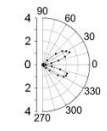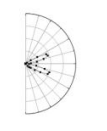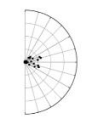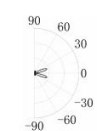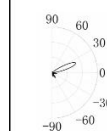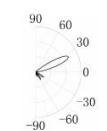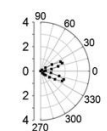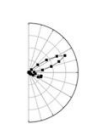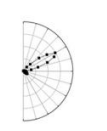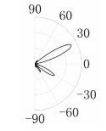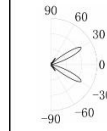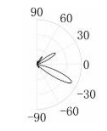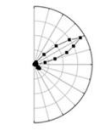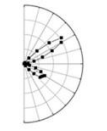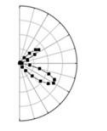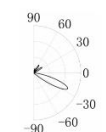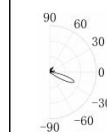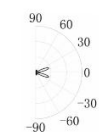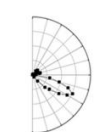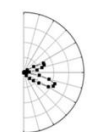
The re-worked TWA model				Our calculations			Reported experiments			
Type	Element factor		Space factor	Current element	In phase	Out of phase	In phase	Out of phase		[10]
Vee bi-filaments	$\left\|\sin(\theta\pm\alpha)\right\|$		$\left\|\dfrac{\sin\left\{\dfrac{kl}{2}[1-\cos(\theta\pm\alpha)]\right\}}{1-\cos(\theta\pm\alpha)}\right\|$							
Type	EF	Array factor	Space factor	Current element	$d=0.5$ mm	2.4 mm	3.4 mm	0.5 mm	2.4 mm	3.4 mm
Parallel bi-filaments	$\left\|\sin\theta\right\|$	$\left\|\cos(\dfrac{kd}{2}\sin\theta-\dfrac{\beta}{2})\right\|$	$\left\|\dfrac{\sin[\dfrac{kl}{2}(1-\cos\theta)]}{1-\cos\theta}\right\|$							
					$\beta=0$	$\pi/4$	$\pi/2$	0 ps	1.7 ps	3.3 ps
					$3\pi/4$	π	$5\pi/4$	3.7 ps	5.3 ps	7.3 ps
					$3\pi/2$	$7\pi/4$	2π	9 ps	10.3 ps	
										[11]

Table III.
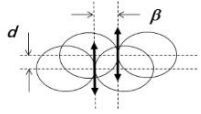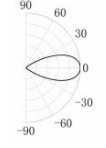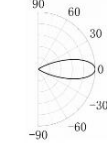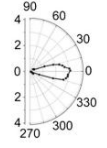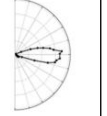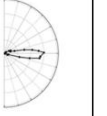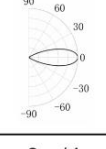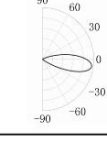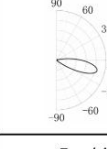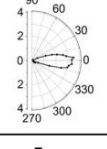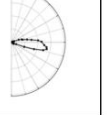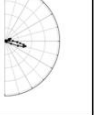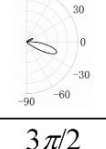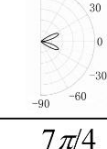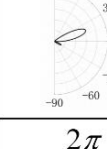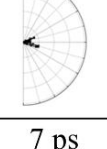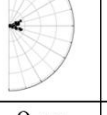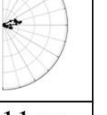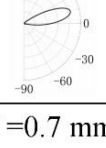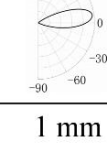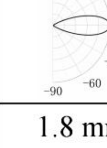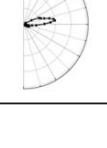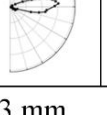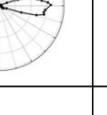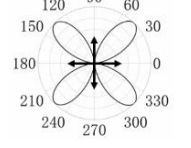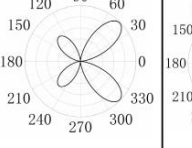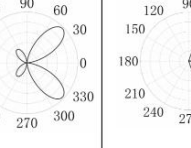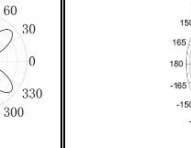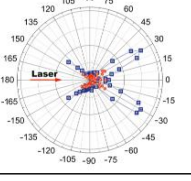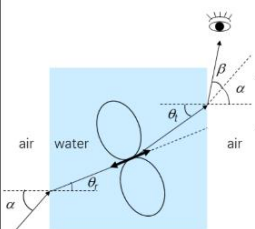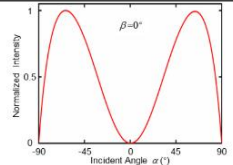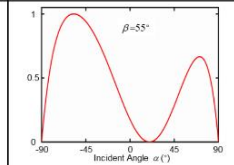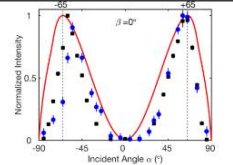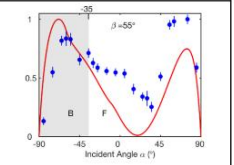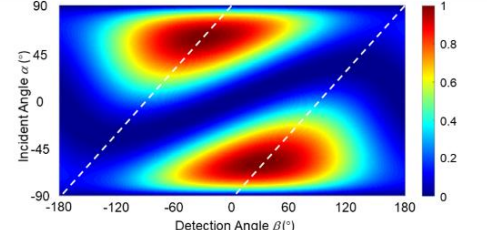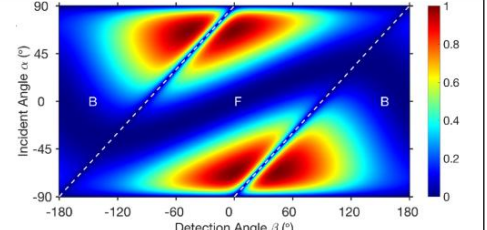
The re-worked TWA model				Our calculations				Reported experiments			
Type	EF	Array factor	Space factor	Current element	$d=1$ mm	2 mm	5 mm	$d=1$ mm	2 mm	5 mm	[12]
Parallel bi-filaments with a transverse DC field	$\left\|\cos\theta\right\|$	$\left\|\cos(\dfrac{kd}{2}\sin\theta-\dfrac{\beta}{2})\right\|$	$\left\|\dfrac{\sin[\dfrac{kl}{2}(1-\cos\theta)]}{1-\cos\theta}\right\|$								
					$\beta=0$	$\pi/4$	$\pi/2$	0 ps	2 ps	4 ps	
					$3\pi/4$	π	$5\pi/4$	5 ps	5.5 ps	6 ps	
					$3\pi/2$	$7\pi/4$	2π	7 ps	9 ps	11 ps	
Type	Element factor			Current element	$l=0.7$ mm	1 mm	1.8 mm	~3 mm			[18]
Single filament with transverse jet of atomic cluster	$\left\|\sin\theta\cdot\cos\theta\right\|$										

Table IV.

The re-worked TWA model			Our calculations				Reported experiments		
Type	EF	Space factor	Current element	$\beta = 0°$		$\beta = 55°$	$\beta = 0°$	$\beta = 55°$	
Micro-filament in the water film	$\left\| \sin(\theta_t + \theta_r) \right\|$	$\left\| \dfrac{\sin\left\{ \dfrac{kl}{2}[1-\cos(\theta_t+\theta_r)] \right\}}{1-\cos(\theta_t+\theta_r)} \right\|$							[17]
	Attenuation factor			$I_{THz}(\alpha, \beta)$			$I_{THz}(\alpha, \beta)$		
	$1 - r^2$								

TABLE I-IV. Formulas for angular distributions of THz emission given by the improved traveling-wave antenna (TWA) model, based on which calculations have been carried out and the results are compared with the reported experimental ones. In the tables, different types of THz sources were taken into account, including a single filament without or with a longitudinal/transverse static electric field, bi-filaments in Vee or parallel shape (without or with a transverse DC field), a micro-filament induced by laser-gas cluster interaction, and a micro-filament created in the water film. Note that, EF in Table II-IV is short for "element factor". The reused figures of experimental results adapted from Ref. [6,9] are with permissions of the corresponding author and American Physical Society; Figures adapted from Ref. [8,11,17,18] are with permissions of AIP Publishing; Figures adapted from Ref. [10] are with pre-permissions of IOP Publishing (formal permissions will be given when this work has a publisher); Figures adapted from Ref. [12] are with permissions of Springer Publishing

3. THZ RESONANCE RADIATION FROM LENGTH-CONTROLLED PLASMA FILAMENTS

3.1 The THz-plasma resonance effect and the corresponding THz spectral peak

According to Section 2, a plasma filament plays similar role of a TWA, which can be treated as a line source with periodic basic current elements. And the total field emission from the antenna is the superposition of waves radiated from individual current element emitters [21]. By this means, the forward radiation profiles of THz wave have been well interpreted as shown in Table I-IV. This, however, seems to mainly solve the THz intensity distributions in the far field, without considering enough details associated with the near-field element emitter. In section 2.2 and 2.3, we briefly mentioned Supplemental Materials A-C by introducing the gain coefficient n and the rotation angle factor φ to the TWA model. These three supplemental sections in fact treated the plasma filament in the microscopic view, thus playing the role of bridging the macroscopic TWA model and the microscopic model.

In microscopic point of view during filamentation, plasma electron oscillations along the plasma filament actually share one physical picture with the current element inside the TWA, e.g., at the beginning and ending points of each plasma dipole oscillation or current element, the moving electron experiencing acceleration and deceleration, respectively [21], as schematically shown in Figure 1(a-b).
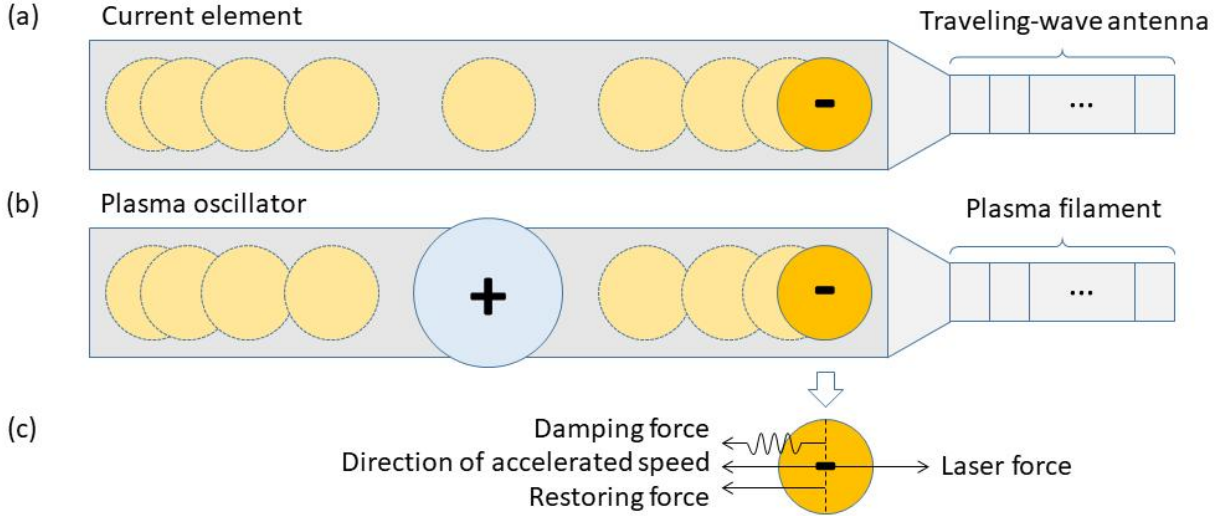
FIGURE 1 Microscopic view between the traveling-wave antenna and the plasma filament. (a) The schematic of a traveling-wave antenna with periodic current elements, inside which the electron (-) gains accelerated velocities at both terminals. (b) Similar case with a plasma filament. At this time, the stationary positive ion (+) is contained inside the elementary plasma oscillator. (c) The force analysis of an electron during plasma oscillation. When the "Restoring force" is solely responsible for driving the "accelerated speed", the "Laser force" energy is then totally converted into "Damping" in form of THz radiation, which then achieves maximum.

Specifically, the process of plasma oscillation can be described as an electron being taken away from the equilibrium position in the post-ionization stage, and the final radiated spectrum is given by (Supplemental Material A)

$$E_{rad}(\omega) \propto i\omega\,\varepsilon_0 E_L \omega_{pe} \frac{\omega + 2iv_e}{2(\omega^2 - \omega_{pe}^2 + iv_e\omega)} \times \frac{\sin(\omega\tau_L/2)}{1-(\omega\tau_L/2\pi)^2} e^{-i\omega\tau_L/2} \tag{3}$$

where $E_L = e\omega_{pe}I_0/2m_e\varepsilon_0 c^2\omega_0^2$ is the amplitude of the plasma wave driven by the laser ponderomotive force, $\omega_{pe} = (N_e e^2/m_e\varepsilon_0)^{1/2}$ is the plasma frequency, v_e is the electron collision frequency and τ_L is the laser pulse duration. One may notice that the first half of Equation (3) (before the multiplication sign) mainly includes parameters relevant to the plasma such as ω_{pe} and v_e, while the second half only involves characteristics of the laser field, e.g., τ_L. Hence, Equation (3) is divided into two parts in the form of $E_{rad}(\omega) \propto E_p(\omega) \times E_l(\omega)$. As for $E_p(\omega)$, it is the spectral component dominated by the plasma parameters in the first half of Equation (3) and can be simplified as:

$$E_p(\omega) \propto i\omega\,\omega_{pe}^2\,\frac{\omega+2i\nu_e}{\omega^2-\omega_{pe}^2+i\nu_e\omega} \tag{4}$$

As for $E_l(\omega)$, it can be written as the following expression:

$$E_l(\omega) \propto \frac{\sin(\omega\tau_L/2)}{1-(\omega\tau_L/2\pi)^2}\,e^{-i\omega\tau_L/2} \tag{5}$$

Next, calculations of the radiated spectra based on Equation (3-5) were performed with typical parameter values: $N_e = 1\times10^{17}$ cm^{-3}, $\lambda = 800$ nm, $\tau_L = 50$ fs, $I_0 = 1\times10^{14}$ W/cm^2 and $\nu_e = 2$ THz. It is worth mentioning that, this ν_e value is supported by both previous publications [3,6,7,9,43,44] and our calculations (Supplemental Material E). It is true that when gases are fully ionized [45], or in case of photo-ionization induced by CEP-stable few-cycle laser pulses [46], the electron collision can be strongly accelerated and $1/\nu_e$ will be even on timescale of 1 fs [46], resulting in $\nu_e \sim 10^3$ THz. However, this is obviously not our condition with air being weakly ionized by multi-cycle laser.

The results are presented in Figure 2(a), in which the total THz radiation given by Equation (3) ($E_{rad}(\omega)$ as the black solid line) is basically the combination of a low-frequency peak given by Equation (4) ($E_p(\omega)$ as the blue dotted line) and high-frequency sinusoidal steps given by Equation (5) ($E_l(\omega)$ as the red dashed line). This hints that the low-frequency peak of $E_{rad}(\omega)$ is mainly associated with the plasma, while the high-frequency sinusoidal steps are decided by the laser field.
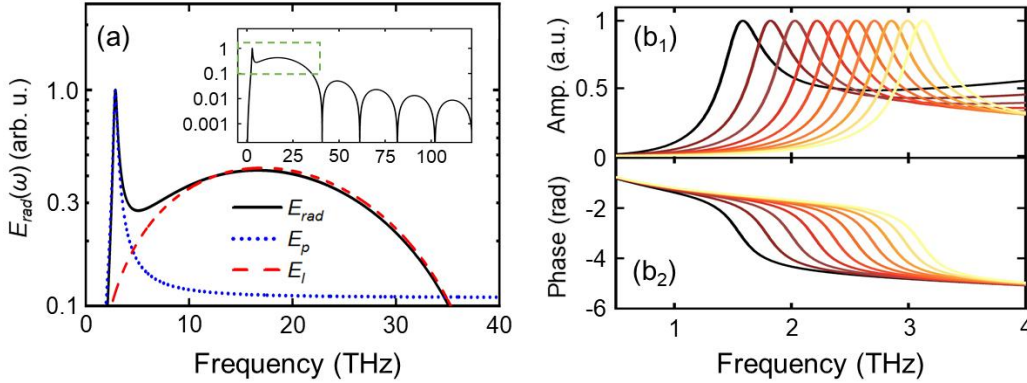
FIGURE 2 **The amplitude and phase spectra of THz radiation given by the resonance effect.** (a) The calculated THz amplitude radiation in frequency domain by Equation (3-5) as the total $E_{rad}(\omega)$ (black solid line), low-frequency $E_p(\omega)$ (blue dotted line) and high-frequency $E_l(\omega)$ (red dashed line), respectively. (a) is enlarged from the green dashed box in its inset, which is the full view of $E_{rad}(\omega)$ along the frequency axis. (b$_1$) The amplitude spectrum of the low-frequency peak as a function of THz frequency with an increasing N_e ranging from 3, 4, 5 ... to 12×10^{16} cm^{-3} (from left to right). (b$_2$) The corresponding spectral phase variations.

The above calculated results agree with theoretical and experimental reports in the literature [13,47], especially for the sinusoidal steps. As for the spectral peak, it actually appears at the plasma frequency $\omega_{pe} = (N_e e^2/m_e\varepsilon_0)^{1/2}$ inside which N_e is the only variable. If increasing N_e from 3×10^{16} to 12×10^{16} cm^{-3}, one can clearly see the blue shift of the spectral peak from 1.6 to 3.2 THz in Figure 2(b$_1$). Homogeneous plasma oscillations were suggested as the source of this spectral maximum at the plasma frequency [23,48,49]. However, these oscillations are theoretically nonradiative [3,50-57]. A question is then naturally raised: what is the origin of this ω_{pe}-dependent THz yield?

By carefully reading Equation (4), the spectral peak could be predicted from the equation's denominator when $\omega_{THz} = \omega_{pe}$, i.e., resonance happens between THz waves and plasma oscillations. In this case, the first two items in Equation (s1,s3,s4) of the Supplemental Material cancel each other, which means that the restoring force eE solely drives the electron oscillation. And thus the laser energy (the fourth item in Equation (s1,s3,s4)) mainly compensates the loss due to the oscillation damping (the third item), which is converted into the THz radiation burst (see also the force analysis in Figure 1(c)). The clue of plasma-THz resonance can also be traced back to Ref. [14], which indicated that (i) the frequency of THz emission varied with the gas density (by changing the

ambient gas pressure) and was close to the bulk plasma frequency as shown in its Figure 3, and (ii) the THz signal was attributed to the nonlinear current in its Equation (1), whose denominator contains the item of [1-$(\omega_{pe}/\omega)^2$]. Both (i) and (ii) reveal that maximum THz signals could be achieved at $\omega_{THz} = \omega_{pe}$ (i.e., resonance effect). It is worth mentioning that, here ω_{pe} is more appropriate than $\omega_{pe}/\sqrt{2}$ or $\omega_{pe}/\sqrt{3}$ for the plasma filament being studied, whose length is significantly larger than its column diameter. Furthermore, spectral phase evolutions corresponding to Figure 2(b$_1$) are shown in Figure 2(b$_2$). Around each peak frequency in Figure 2(b$_1$), phase variations of π (3.14 in rad) can be observed in Figure 2(b$_2$), further verifying the THz-plasma resonance effect. In the following section, superpositions of this elementary resonance radiation of THz wave along a single-color filament would be discussed.

3.2 Indication of the resonance effect: temporally periodic oscillation and its phase variation

Along a photo-ionization induced plasma filament in air, the longitudinal plasma density N_e distribution can be simulated by the nonlinear wave equation considering the slowly varying envelope approximation [58]:

$$2ik_0\frac{\partial A}{\partial z} + \Delta_\perp A + 2(1 + \frac{i}{\omega}\frac{\partial}{\partial \tau})\frac{k_0^2}{n_0}(\Delta n_{Kerr} + \Delta n_{plasma})A - k_2 k_0 \frac{\partial^2 A}{\partial t^2} - ik_0 \alpha A = 0 \qquad (6)$$

Equation (6) contains several optical effects, including self-focusing, diffraction, group-velocity dispersion, and plasma generation due to multi-photon-tunnel ionization, etc. Here, k_0 and k_2 represent wave number and group velocity dispersion parameter, respectively. α is the absorption coefficiency associated with ionization in air. And A is the electric field envelope function. The following initial parameters were adopted for simulations of N_e: 50 fs, 800 nm, 1 kHz and 1 W laser pulses were focused by a lens with $f = 100$ cm.

The simulated on-axis distribution of N_e along the filament is shown in Figure 3(a). The maximum of N_e appears at $z = 0$ mm which is defined as the focal point of the laser. Note that, the plasma could be produced within the same temporal scale of the pumping laser pulse duration, e.g., a few tens of femtoseconds [59], while the plasma's average lifetime is as long as several nanoseconds [60]. This fact hints that, the plasma could be formed in an instant moment before the THz pulse generation. Afterwards, it would last enough long time for THz-plasma interactions. For this reason, we paid little attention on the temporal evolution of N_e in the following treatments. Based on the N_e evolution in Figure 3(a) and Equation (3) of $E_{rad}(\omega)$, 2-D THz amplitude distribution as functions of z and THz frequency were calculated and displayed in Figure 3(b). One can see that three horizontal dark-color areas within 80 THz correspond to the first three sinusoidal steps like that in the inset of Figure 2(a). And the low-frequency component (< 4 THz) in the dashed black box is further enlarged and presented in the inset of Figure 3(b), in which the spectral peak frequency increases first and then decreases. This peak frequency variation follows the N_e evolution (in Figure 3(a)) as previously illustrated in Figure 2(b$_1$).
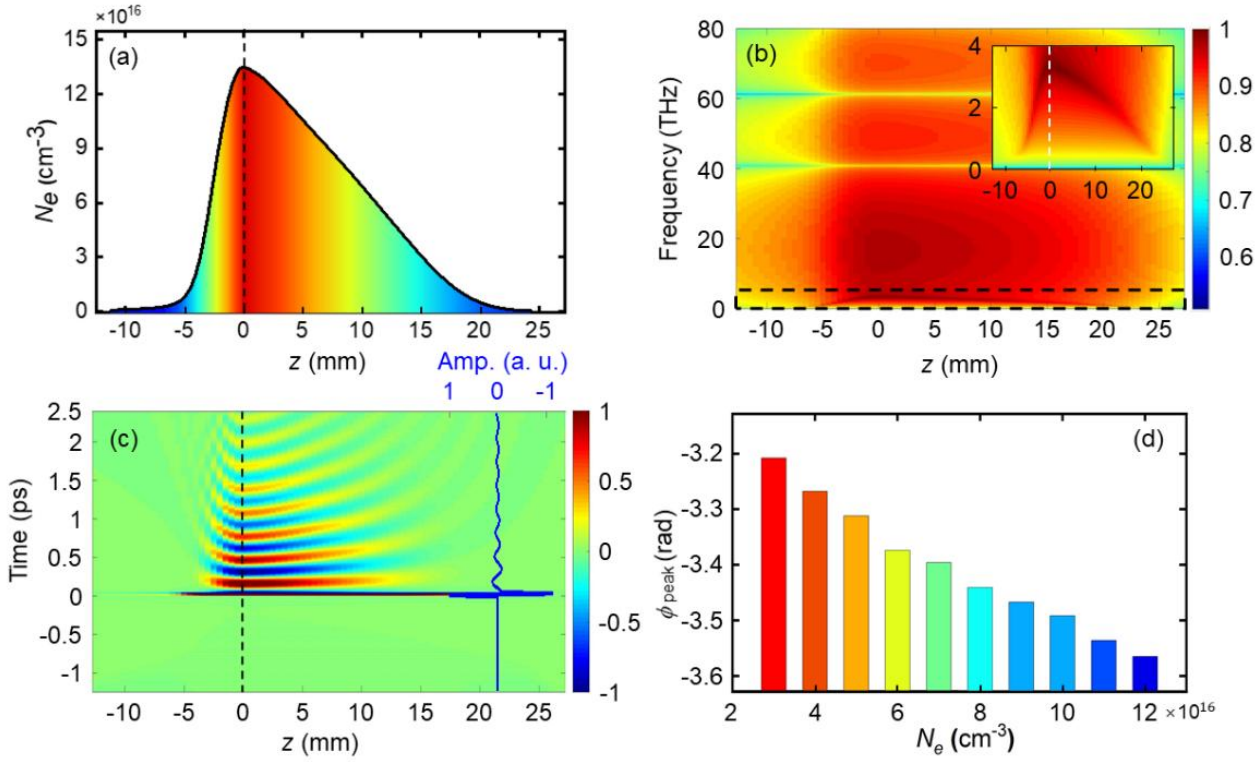
FIGURE 3 THz signals in both time and frequency domains along the plasma filament with an inhomogeneous N_e distribution. (a) The simulated longitudinal N_e distribution along the propagation axis z of the plasma filament. (b) 2-D THz amplitude distributions as functions of z and THz frequency. Inset: the enlarged view of low THz band (<4 THz) within the black dashed box. (c) 2-D THz amplitude distributions as functions of z and time delay, achieved by inverse Fourier Transformations (iFT) on (b). The blue waveform on the right-hand side, given by z-integration, denotes the THz transient emitted from the entire plasma filament. (d) The phase of spectral peak (ϕ_{peak}) decreases with the increasing N_e, obtained from Figure 2(b$_2$).

In next step, inverse Fourier Transformations (iFT) were performed on the data in Figure 3(b), and the corresponding results are shown in Figure 3(c) as 2-D THz temporal waveforms with respect to z. In the right side of Figure 3(c), the blue THz waveform is given by z-integration of the 2-D data. Theoretically, sinusoidal steps and spectral peaks in Figure 3(b) are expected to be iF-transformed into single-cycle pulses and periodic oscillations in time domain, respectively. This is actually what can be seen in Figure 3(c): the single-cycle main pulse of THz radiation is located around $t = 0$ ps, and periodic oscillations are after the THz main pulse along the time axis.

It can also be noticed in Figure 3(c) that 2-D "stripes" bend at the vicinity of $z = 0$ mm. Now, attentions were focused on this bending phenomenon, which in fact indicates temporal advance (before $z = 0$ mm) and delay (after $z = 0$ mm) of the periodic oscillation. In other words, the phase of temporal oscillations (at spectral peak frequency) decreased first (before $z = 0$ mm) and then increased (after $z = 0$ mm). On the other hand, one can see in Figure 3(a) that N_e increased and decreased before and after $z = 0$ mm, respectively. Thus, the growth of N_e might contribute to the phase decreasing at the spectral peak frequency, and vice versa. This hypothesis has been proved by extracting the phase value at peak frequency under different N_e in Figure 2(b$_2$) and plotting the results in Figure 3(d), in which the spectral peak's phase is in anti-correlation relationship with N_e as expected.

3.3 Distortion of the temporal oscillations due to the limited bandwidth of the THz detection system

The above temporally periodic oscillation after the main THz pulse, and its phase variations with respect to N_e, are rarely reported in previous publications. Possible reasons are discussed in this section. In experiments, the plasma filament generated by focusing femtosecond laser pulses in air usually has a plasma density N_e greater than 10^{16} cm^{-3} [61]. Therefore, the corresponding resonance frequency ($\omega_{pe}/2\pi$) is > 0.89 THz. Coincidentally, this frequency value is close to the upper cut-off frequency of the constantly used ZnTe crystal in the traditional electro-optic (EO) sampling setup for temporal THz waveforms detection. For example, an 1.5-mm-thick ZnTe crystal has an upper cut-off frequency no more than 1 THz [62], beyond which the THz spectral signal would be

seriously attenuated by the material phonon absorption. Accordingly, the proposed spectral resonance peaks along the plasma filament (in Figure 3(b)) are very likely to be erased due to this finite bandwidth of the EO crystal, especially around the laser focus where ω_{pe} is relatively larger.

Consider the response function of a ZnTe crystal as a shifted Gaussian function of $R(f) = \exp[-2(f-f_0)^2/\Delta f^2]$, where $(f_0, \Delta f)$ are set to be (0.2, 1.6), (0.1, 0.8) and (0.05, 0.4) THz in the following studies. Thus the corresponding upper cutoff frequencies at $1/e^2$ of the Gaussian distributions are about 1.8, 0.9 and 0.45 THz, respectively. These response functions for low-pass filtering are shown in the left-hand side of Figure 4(a_1-a_3) as white lines, and the main part of Figure 4(a_1-a_3) are the filtered 2-D THz distributions achieved by multiplying the response functions with the data originally shown in the inset of Figure 3(b). One can see in Figure 4(a_1) that the spectral peaks around $z = 0$ mm have been filtered out, and this phenomenon is even more serious in Figure 4(a_2-a_3) due to the narrowed window width. Meanwhile in time domain as shown in Figure 4(b_1-b_3), this low-pass filtering effect mainly reduces the "stripe" bending around $z = 0$ mm, where temporal advance or delay can no longer be observed. Furthermore, the main THz single-cycle pulse and the following periodic oscillations gradually combine into a slowly-varying waveform, whose duration gets much wider towards Figure 4(b_3).
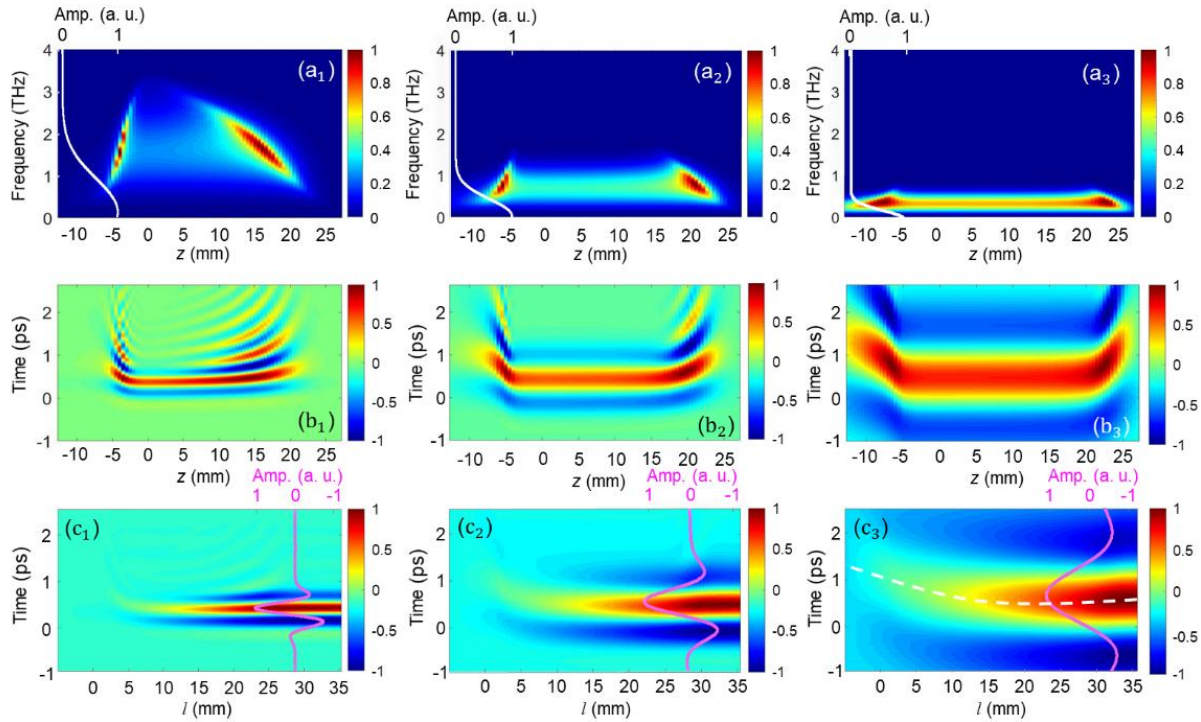
FIGURE 4 The temporal THz waveforms detected with different bandwidths. (a) The low-pass filtered results of 2-D THz spectrum distributions, achieved by multiplying the data in Figure 3(b) by the window functions (white lines) overlapped on the left side of (a_1-a_3), whose upper cutoff frequencies (at $1/e^2$) are 1.8, 0.9 and 0.45 THz, respectively. (b) The corresponding 2-D THz distributions in time domain at each point z. (c) The integrated outcomes of (b) as a function of the filament length l. The purple lines highlight the final THz waveforms from the whole plasma filament.

Figure 4(a_1-a_3) and 4(b_1-b_3) display the THz spectral and temporal signals generated at each z position. In actual experiments, the directly detected data should be the coherent combination of pulses along the plasma filament with a certain length. Moreover, this length can be controlled by inserting a blocker (perpendicularly to the z axis) inside the filament [63]. Therefore, the THz waveforms in time domain as shown in Figure 4(b_1-b_3) were integrated as a function of z, and the calculated consequences are presented in Figure 4(c_1-c_3). It can be seen that at the leading end of the filament ($l < 10$ mm), there is a temporally forward shift of THz pulses. Nevertheless, this trend is no longer evident in case of $l > 10$ mm, where the displacement of the waveform maximum tends to be a constant. THz waveforms at $l = 35$ mm as final signals radiated from the whole plasma filaments are extracted and plotted on the right-hand side of Figure 4(c_1-c_3) as purple lines. One can clearly see the missing of temporally periodic oscillations after the main THz pulse (in comparison with Figure 3(c)). In this situation, only the temporal advance of THz pulses at the front end of the filament could account for the occurrence of the THz-plasma resonance. This tendency has been illustrated by a white dashed curve in Figure 4(c_3), which

highlights the time-domain locations of the maximum THz amplitude, and would also be experimentally verified in the next section.

3.4 Experimental demonstrations of the THz-plasma resonance effect by observing the temporal advance phenomenon

In this section, experiments have been carried out in order to confirm the theoretical predictions about the temporal advance of THz waveforms in Figure 4(c_1-c_3) as the indirect evidence for the resonance behavior between THz and plasma waves. Thus, the laser equipment operated with the same parameters as described in Section 3.2 for THz wave generation during filamentation in the air. Specifically, the blocker used for varying the filament length was a ceramic plate in thickness of about 0.8 mm [64]. In addition, the detection setup adopted the typical THz-TDS scheme [65], in which a 1.5-mm-thick ZnTe crystal was adopted for EO sampling. Finally, temporal THz waveforms radiated from length-controlled filaments were detected.

The experimental results are shown in Figure 5(a), whose differential outcomes are indicated in Figure 5(b). Both figures well reproduced the computed temporal shift of the single-cycle THz pulse as displayed in Figure 4(c_3) and (b_3), respectively. Figure 5(c) further quantified the displacements of the THz waveform maximums along the dashed white lines in Figure 5(a) and Figure 4(c_3), as red circles and black line, respectively, and their fitting with each other is acceptable. Note that in Figure 5(c) the red open circles have been shifted as a whole along the ps-axis (for better comparison with the black line), which is reasonable since the temporal zero point of the detected THz waveform via the pump-probe method is arbitrary.
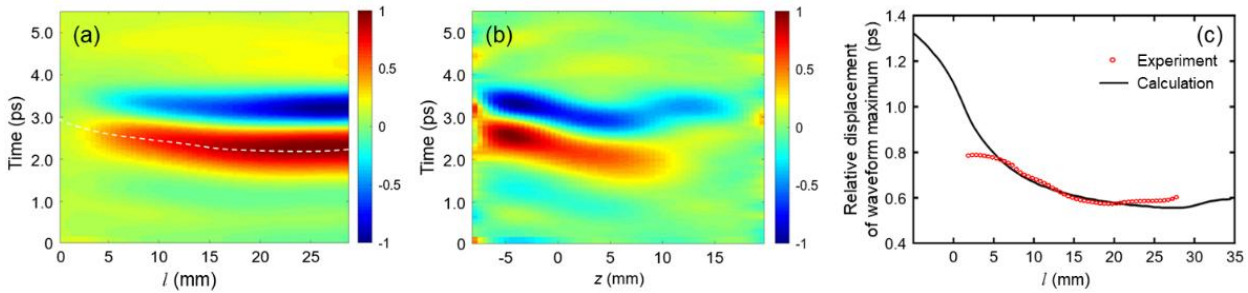
FIGURE 5 Comparison between the experimental and theoretical results of THz wave temporal shift. (a) The recorded THz waveforms emitted from different filament lengths l. (b) THz pulses generated at each z position, achieved by applying differential on the data in (a). (c) The relative displacement of the temporal waveform maximum obtained from Figure 4(c_3) as the black line, and from Figure 5(a) as the red circles. Note that, the latter was offset along the ps-axis for fitting with the former.

It is also worthy of mentioning that, our scheme of recording the temporally advanced THz waveforms (in Figure 5(a)) is a compromise since few candidates are available. One may prefer to directly detect the sharp peak of THz spectrum located at ω_p (in Figure 2(a)) or the equivalent periodic oscillations in time domain (in Figure 3(c)) by using a broadband EO crystal. However, both methods might not be practical for the following reasons. Firstly, ω_p is determined by N_e which varies along the filament (Figure 3(a)), and thus the overall THz spectral maximum (centered at ω_p) of the entire filament cannot be such a "sharp" peak like that in Figure 2(a) calculated at a certain N_e value. Normally, a much smooth ω_p peak is reported in the literature [23,48,49]. Secondly, as for the temporal periodic oscillation, it should be mixed with different frequency components because its FT-related ω_p peak has a considerable bandwidth as mentioned above. Besides, it is well known that the water vapor absorption in air contributes to the random fluctuation of THz amplitude after the main monocycle pulse [66]. These two points would inevitably hinder the expected periodic oscillation from being identified.

4. CONCLUSION

In summary, the current work has provided a new insight into the THz wave generation during single-color femtosecond laser filamentation in gaseous or liquid media with the improved TWA model. On one hand, representative far-field THz radiation profiles observed in experiments of previous publications [6,8-12,17,18], such as (a)symmetrical conical or on-axis THz beam propagation, have been well reproduced with our TWA theory. On the other hand, the plasma electron oscillations have been uncovered as periodic THz emitters along

the filament via the effect of THz-plasma resonance, and the temporal advance of THz waveforms is proposed as the practical evidence for the existence of this effect. Owing to the above issues, the underlying nature of THz wave creation by the single-color laser field is approaching to be thoroughly understood in a novel viewpoint of radiated antennas.

Notice that, the suggested TWA perspective is particularly associated with the single-color laser field driven longitudinal photoionization currents. In contrast, a two-color laser driver is commonly understood in terms of transverse currents [67,68]. However, studies of two- [59,69] or even multi-color [70-74] laser pumping THz sources, as well as the phased-array plasma filament emitters, might also benefit from the TWA theory. Since it has been discovered that both transverse and longitudinal currents contribute to the THz emission during filamentation [3,53,75-81], and the longitudinal currents tend to become dominant within specific ranges of parameters, like gas pressures, pumping wavelengths, and laser intensities [22,82,83]. Therefore, the suggested TWA model is very promising to show its versatility far beyond what has been presented in this work.

Funding:

Competing interests:

The author(s) declare(s) that there is no conflict of interest regarding the publication of this article.

Author contributions:

J.Z. and Y.P. conceived the idea and designed the experiments. Y.H. and Y.C. performed the experiments with help from Z.J. Y.H. and A.P.S. discussed the experimental results. Simulations were performed by J.Z. and Y.H. All authors wrote the manuscript. Y.Z. and S.Z. supervised the project.

REFERENCES

[1] PA. C.R. Cherenkov, Acad. Sci. U.S.S.R. 2:451 (1934).

[2] Frank I, Tamm ICR. Acad. Sci U.S.S.R. 14:109 (1937).

[3] P. Sprangle, J. R. Penano, B. Hafizi, and C. A. Kapetanakos, Ultrashort laser pulses and electromagnetic pulse generation in air and on dielectric surfaces, Phys. Rev. E 69, 066415 (2004). https://doi.org/10.1103/PhysRevE.69.066415.

[4] J. Zheng, C. X. Yu, Z. J. Zheng, and K. A. Tanaka, Cherenkov radiation generated by a beam of electrons revisited, Phys. Plasmas 12, 093105 (2005). https://doi.org/10.1063/1.2040178.

[5] J. Ružička, V. P. Zrelov, Optical transition-radiation in a transparent medium and its relation to the Vavilov-Cherenkov radiation, Czech. J. Phys. 43(5), 551-567 (1993). https://doi.org/10.1007/BF01589740.

[6] C. D'Amico, A. Houard, M. Franco, B. Prade, A. Mysyrowicz, A. Couairon, and V. T. Tikhonchuk, Conical forward THz emission from femtosecond-laser-beam filamentation in air, Phys. Rev. Lett. 98, 235002 (2007). https://doi.org/10.1103/PhysRevLett.98.235002.

[7] C. D'Amico, A. Houard, S. Akturk, Y. Liu, J. Le Bloas, M. Franco, B. Prade, A. Couairon, V. T. Tikhonchuk, and A. Mysyrowicz, Forward THz radiation emission by femtosecond filamentation in gases: theory and experiment, New J. Phys. 10, 013015 (2008). https://doi.org/10.1088/1367-2630/10/1/013015.

[8] Y. Liu, A. Houard, B. Prade, A. Mysyrowicz, A. Diaw, and V. T. Tikhonchuk, Amplification of transition-Cherenkov terahertz radiation of femtosecond filament in air, Appl. Phys. Lett. 93, 051108 (2008). https://doi.org/10.1063/1.2965612.

[9] A. Houard, Y. Liu, B. Prade, V. T. Tikhonchuk, and A. Mysyrowicz, Strong enhancement of terahertz radiation from laser filaments in air by a static electric field, Phys. Rev. Lett. 100, 255006 (2008). https://doi.org/10.1103/PhysRevLett.100.255006.

[10] S. I. Mitryukovskiy, Y. Liu, B. Prade, A. Houard, and A. Mysyrowicz, Coherent interaction between the terahertz radiation emitted by filaments in air, Laser Phys. 24, 094009 (2014). https://doi.org/10.1088/1054-660X/24/9/094009.

[11] S. I. Mitryukovskiy, Y. Liu, B. Prade, A. Houard, and A. Mysyrowicz, Coherent synthesis of terahertz radiation from femtosecond laser filaments in air, Appl. Phys. Lett. 102, 221107 (2013). https://doi.org/10.1063/1.4807917.

[12] S. I. Mitryukovskiy, Y. Liu, B. Prade, A. Houard, and A. Mysyrowicz, Effect of an external electric field on the coherent terahertz emission from multiple filaments in air, Appl. Phys. B 117, 265-269 (2014). https://doi.org/10.1007/s00340-014-5830-1.

[13] G.-Y. Hu, B. Shen, A.-L. Lei, R.-X. Li, and Z.-Z. Xu, Transition-Cherenkov radiation of terahertz generated by super-luminous ionization front in femtosecond laser filament, Laser Part. Beams 28, 399-407 (2010). https://doi.org/10.1017/S0263034610000388.

[14] H. Hamster, A. Sullivan, S. Gordon, W. White, and R. W. Falcone, Subpicosecond, electromagnetic pulses from intense laser-plasma interaction, Phys. Rev. Lett. 71, 2725-2728 (1993). https://doi.org/10.1103/PhysRevLett.71.2725.

[15] S. N. Galyamin, A. V. Tyukhtin, A. Kanareykin, and P. Schoessow, Reversed Cherenkov-transition radiation by a charge crossing a left-handed medium boundary, Phys. Rev. Lett. 103, 194802 (2009). https://doi.org/10.1103/PhysRevLett.103.194802.

[16] X. Lin, S. Easo, Y. Shen, H. Chen, B. Zhang, J. D. Joannopoulos, M. Soljačić, and I. Kaminer, Controlling Cherenkov angles with resonance transition radiation, Nat. Phys. 14, 816-821 (2018). https://doi.org/10.1038/s41567-018-0138-4.

[17] Y. E, Q. Jin, A. Tcypkin, and X.-C. Zhang, Terahertz wave generation from liquid water films via laser-induced breakdown, Appl. Phys. Lett. 113, 181103 (2018). https://doi.org/10.1063/1.5054599.

[18] F. Jahangiri, M. Hashida, T. Nagashima, S. Tokita, M. Hangyo, and S. Sakabe, Intense terahertz emission from atomic cluster plasma

produced by intense femtosecond laser pulses, Appl. Phys. Lett. 99, 261503 (2011). https://doi.org/10.1063/1.3672814.

[19] Balanis Constantine, Antenna theory analysis and design, John Wiley & Sons, Inc. USA, 2005, 169-357. ISBN: 047166782X.

[20] G. S. Smith, Teaching antenna radiation from a time-domain perspective, Am. J. Phys. 69, 288-300 (2001). https://doi.org/10.1119/1.1320439.

[21] G. S. Smith, On the Interpretation for Radiation from Simple Current Distributions, IEEE Antenn. Propag. M. 40(4), 39-44 (1998). https://doi.org/10.1109/74.730536.

[22] A. M. Zheltikov, Laser filaments as pulsed antennas, Opt. Lett. 46, 4984-4987 (2021). https://doi.org/10.1364/OL.426023.

[23] V. A. Andreeva, O. G. Kosareva, N. A. Panov, D. E. Shipilo, P. M. Solyankin, M. N. Esaulkov, P. Gonzalez de Alaiza Martinez, A. P. Shkurinov, V. A. Makarov, L. Berge, and S. L. Chin, Ultrabroad Terahertz Spectrum Generation from an Air-Based Filament Plasma, Phys. Rev. Lett. 116, 063902 (2016). https://doi.org/10.1103/PhysRevLett.116.063902.

[24] V. Borodin, N. A. Panov, O. G. Kosareva, V. A. Andreeva, M. N. Esaulkov, V. A. Makarov, A. P. Shkurinov, S. L. Chin, and X.-C. Zhang, Transformation of terahertz spectra emitted from dual-frequency femtosecond pulse interaction in gases, Opt. Lett. 38, 1906-1908 (2013). https://doi.org/10.1364/OL.38.001906.

[25] J. Zhao, W. Liu, S. Li, D. Lu, Y. Zhang, Y. Peng, Y. Zhu, and S. Zhuang, Clue to a thorough understanding of terahertz pulse generation by femtosecond laser filamentation, Photonics Res. 6, 296 (2018). https://doi.org/10.1364/PRJ.6.000296.

[26] H. Wang, and T. Shen, Unified theoretical model for both one- and two-color laser excitation of terahertz waves from a liquid, Appl. Phys. Lett. 117, 131101 (2020). https://doi.org/10.1063/5.0014872.

[27] J. D Kraus. and, R. J. Marhefka, Antennas: For All Applications, 3rd Edition, McGraw-Hill Publication, Boston, 2008, 232-233, ISBN: 9780072321036.

[28] F. Buccheri, and X.-C. Zhang, Terahertz emission from laser-induced microplasma in ambient air, Optica 2, 366 (2015). https://doi.org/10.1364/OPTICA.2.000366.

[29] H. Zhao, Y. Tan, L. Zhang, R. Zhang, M. Shalaby, C. Zhang, Y. Zhao, and X.-C. Zhang, Ultrafast hydrogen bond dynamics of liquid water revealed by terahertz-induced transient birefringence, Light Sci. Appl. 9, 136 (2020). https://doi.org/10.1038/s41377-020-00370-z.

[30] L.-L. Zhang, W.-M. Wang, T. Wu, S.-J. Feng, K. Kang, C.-L. Zhang, Y. Zhang, Y.-T. Li, Z.-M. Sheng, and X.-C. Zhang, Strong Terahertz Radiation from a Liquid-Water Line, Phys. Rev. Appl. 12, 014005 (2019). https://doi.org/10.1103/PhysRevApplied.12.014005.

[31] Y. E, Q. Jin, and X.-C. Zhang, Enhancement of terahertz emission by a preformed plasma in liquid water, Appl. Phys. Lett. 115, 101101 (2019). https://doi.org/10.1063/1.5119812.

[32] Q. Jin, J. Dai, Y. E, and X.-C. Zhang, Terahertz wave emission from a liquid water film under the excitation of asymmetric optical fields, Appl. Phys. Lett. 113(26), 261101 (2018). https://doi.org/10.1063/1.5064644.

[33] Q. Jin, Y. E, K. Williams, J. Dai, and X.-C. Zhang, Observation of broadband terahertz wave generation from liquid water, Appl. Phys. Lett. 111, 071103 (2017). https://doi.org/10.1063/1.4990824.

[34] E. A. Ponomareva, A. N. Tcypkin, S. V. Smirnov, S. E. Putilin, E. Yiwen, S. A. Kozlov, and X.-C. Zhang, Double-pump technique - one step closer towards efficient liquid-based THz sources, Opt. Express 27, 32855-32862 (2019). https://doi.org/10.1364/OE.27.032855.

[35] N. Tcypkin, E. A. Ponomareva, S. E. Putilin, S. V. Smirnov, S. A. Shtumpf, M. V. Melnik, Y. E, S. A. Kozlov, and X.-C. Zhang, Flat liquid jet as a highly efficient source of terahertz radiation, Opt. Express 27, 15485-15494 (2019). https://doi.org/10.1364/OE.27.015485.

[36] N. Tcypkin, M. V. Melnik, M. O. Zhukova, I. O. Vorontsova, S. E. Putilin, S. A. Kozlov, and X.-C. Zhang, High Kerr nonlinearity of water in THz spectral range, Opt. Express 27, 10419-10425 (2019). https://doi.org/10.1364/OE.27.010419.

[37] I. Dey, K. Jana, V. Y. Fedorov, A. D. Koulouklidis, A. Mondal, M. Shaikh, D. Sarkar, A. D. Lad, S. Tzortzakis, A. Couairon, and G. R. Kumar, Highly efficient broadband terahertz generation from ultrashort laser filamentation in liquids, Nat. Commun. 8, 1184 (2017). https://doi.org/10.1038/s41467-017-01382-x.

[38] Y. E, Y. Cao, F. Ling, and X.-C. Zhang, Flowing cryogenic liquid target for terahertz wave generation, AIP Adv. 10, 105119 (2020). https://doi.org/10.1063/5.0023106.

[39] V. Balakin, J.-L. Coutaz, V. A. Makarov, I. A. Kotelnikov, Y. Peng, P. M. Solyankin, Y. Zhu, and A. P. Shkurinov, Terahertz wave generation from liquid nitrogen, Photonics Res. 7, 678 (2019). https://doi.org/10.1364/PRJ.7.000678.

[40] Y. Cao, Y. E, P. Huang, and X.-C. Zhang, Broadband terahertz wave emission from liquid metal, Appl. Phys. Lett. 117, 041107 (2020). https://doi.org/10.1063/5.0015507.

[41] P. M. Solyankin, B. V. Lakatosh, M. S. Krivokorytov, I. P. Tsygvintsev, A. S. Sinko, I. A. Kotelnikov, V. A. Makarov, J.-L. Coutaz, V. V. Medvedev, and A. P. Shkurinov, Single Free-Falling Droplet of Liquid Metal as a Source of Directional Terahertz Radiation, Phys. Rev. Appl. 14, 034033 (2020). https://doi.org/10.1103/PhysRevApplied.14.034033.

[42] K. J. Garriga Francis, M. Lim Pac Chong, Y. E, and X.-C. Zhang, Terahertz nonlinear index extraction via full-phase analysis, Opt. Lett. 45, 5628-5631 (2020). https://doi.org/10.1364/OL.399999.

[43] M. Alshershby, Z. Hao, and J. Lin, Guiding microwave radiation using laser-induced filaments: the hollow conducting waveguide concept, J. Phys. D: Appl. Phys. 45, 265401 (2012). https://doi.org/10.1088/0022-3727/45/26/265401.

[44] R. R. Musin, M. N. Shneider, A. M. Zheltikov, and R. B. Miles, Guiding radar signals by arrays of laser-induced filaments: finite-difference analysis, Appl. Opt. 46, 5593-5597 (2007). https://doi.org/10.1364/AO.46.005593.

[45] Lyman Spitzer Jr., Physics of Fully Ionized Gases, Dover Publications, USA, 2006, ISBN: 9780486449821.

[46] M. Kreß, T. Löffler, M. D. Thomson, R. Dörner, H. Gimpel, K. Zrost, T. Ergler, R. Moshammer, U. Morgner, J. Ullrich, and H. G. Roskos, Determination of the carrier-envelope phase of few-cycle laser pulses with terahertz-emission spectroscopy, Nat. Phys. 2, 327–331(2006). https://doi.org/10.1038/nphys286.

[47] B. Forestier, A. Houard, M. Durand, Y. B. André, B. Prade, J. Y. Dauvignac, F. Perret, C. Pichot, M. Pellet, and A. Mysyrowicz, Radiofrequency conical emission from femtosecond filaments in air, Appl. Phys. Lett. 96, 141111 (2010). https://doi.org/10.1063/1.3378266.

[48] H. Hamster, A. Sullivan, S. Gordon, and R. W. Falcone, Short-pulse terahertz radiation from high-intensity-laser-produced plasmas, Phys. Rev. E 49, 671-677 (1994). https://doi.org/10.1103/PhysRevE.49.671.

[49] N. Li, Y. Bai, T. Miao, P. Liu, R. Li and Z. Xu, Revealing plasma oscillation in THz spectrum from laser plasma of molecular jet, Opt. Express, 24(20), 23009-23017 (2016). https://doi.org/10.1364/OE.24.023009.

[50] V. T. Tikhonchuk, Comment on "Generation of Electromagnetic Pulses from Plasma Channels Induced by Femtosecond Light Strings", Phys. Rev. Lett. 89, 209301 (2002). https://doi.org/10.1103/PhysRevLett.89.209301.

[51] M. Bystrov, N. V. Vvedenskii and V. B. Gildenburg, Generation of terahertz radiation upon the optical breakdown of a gas, J. Exp. Theor. Phys, 82(12), 753-757 (2005). https://doi.org/10.1134/1.2175243.

[52] V. B. Gildenburg, and N. V. Vvedenskii, Optical-to-THz wave conversion via excitation of plasma oscillations in the tunneling-ionization process, Phys. Rev. Lett. 98, 245002 (2007). https://doi.org/10.1103/PhysRevLett.98.245002.

[53] I. Thiele, R. Nuter, B. Bousquet, V. Tikhonchuk, S. Skupin, X. Davoine, L. Gremillet, and L. Berge, Theory of terahertz emission from femtosecond-laser-induced microplasmas, Phys. Rev. E 94, 063202 (2016). https://doi.org/10.1103/PhysRevE.94.063202.

[54] L. M. Gorbunov and A. A. Frolov, Transition radiation generated by a short laser pulse at a plasma-vacuum interface, Plasma Phys. Rep. 32, 850-865 (2006). https://doi.org/10.1134/S1063780X06100059.

[55] P. González de Alaiza Martinez, X. Davoine, A. Debayle, L. Gremillet, and L. Berge, Terahertz radiation driven by two-color laser pulses at near-relativistic intensities: Competition between photoionization and wakefield effects, Sci. Rep. 6, 26743 (2016). https://doi.org/10.1038/srep26743.

[56] C. Miao, J. P. Palastro, and T. M. Antonsen, Laser pulse driven terahertz generation via resonant transition radiation in inhomogeneous plasmas, Phys. Plasmas 23, 063103 (2016). https://doi.org/10.1063/1.4953098.

[57] I. Thiele, B. Zhou, A. Nguyen, E. Smetanina, R. Nuter, K. J. Kaltenecker, P. González de Alaiza Martínez, J. Déchard, L. Bergé, P. U. Jepsen, and S. Skupin, Terahertz emission from laser-driven gas plasmas: a plasmonic point of view, Optica 5, 1617 (2018). https://doi.org/10.1364/OPTICA.5.001617.

[58] B. Zeng, W. Chu, H. Gao, W. Liu, G. Li, H. Zhang, J. Yao, J. Ni, S. L. Chin, Y. Cheng, and Z. Xu, Enhancement of peak intensity in a filament core with spatiotemporally focused femtosecond laser pulses, Phys. Rev. A 84, 063819 (2011). https://doi.org/10.1103/PhysRevA.84.063819.

[59] K. Y. Kim, J. H. Glownia, A. J. Taylor, and G. Rodriguez, Terahertz emission from ultrafast ionizing air in symmetry-broken laser fields, Opt. Express, 15(8), 4577–4584 (2007). https://doi.org/10.1364/OE.15.004577.

[60] A. Couairon and A. Mysyrowicz, Femtosecond filamentation in transparent media, Phys. Rep. 441, 47–189 (2007). https://doi.org/10.1016/j.physrep.2006.12.005.

[61] F. Theberge, W. Liu, P. T. Simard, A. Becker, and S. L. Chin, Plasma density inside a femtosecond laser filament in air: strong dependence on external focusing, Phys. Rev. E 74, 036406 (2006). https://doi.org/10.1103/PhysRevE.74.036406.

[62] A. Leitenstorfer, S. Hunsche, J. Shah, M. C. Nuss, and W. H. Knox, Detectors and sources for ultrabroadband electro-optic sampling: Experiment and theory, Appl. Phys. Lett. 74, 1516-1518 (1999). https://doi.org/10.1063/1.123601.

[63] Y. Bai, L. Song, R. Xu, C. Li, P. Liu, Z. Zeng, Z. Zhang, H. Lu, R. Li, and Z. Xu, Waveform-Controlled Terahertz Radiation from the Air Filament Produced by Few-Cycle Laser Pulses, Phys. Rev. Lett. 108(25), 255004 (2012). https://doi.org/10.1103/PhysRevLett.108.255004.

[64] J. Zhao, W. Chu, L. Guo, Z. Wang, J. Yang, W. Liu, Y. Cheng, and Z. Xu, Terahertz imaging with sub-wavelength resolution by femtosecond laser filament in air, Sci. Rep. 4, 3880 (2014). https://doi.org/10.1038/srep03880.

[65] M. Tonouchi, Cutting-edge terahertz technology, Nat. photonics 1(2), 97-105 (2007). https://doi.org/10.1038/nphoton.2007.3

[66] J. Liu, J. Dai, S. L. Chin, and X.-C. Zhang, Broadband terahertz wave remote sensing using coherent manipulation of fluorescence from asymmetrically ionized gases, Nat. Photonics 4, 627-631 (2010). https://doi.org/10.1038/nphoton.2010.165.

[67] K. Y. Kim, A. J. Taylor, J. H. Glownia, and G. Rodriguez, Coherent control of terahertz supercontinuum generation in ultrafast laser–gas interactions, Nat. Photonics 2, 605-609 (2008). https://doi.org/10.1038/nphoton.2008.153.

[68] I. Babushkin, W. Kuehn, C. Köhler, S. Skupin, L. Bergé, K. Reimann, M. Woerner, J. Herrmann, and T. Elsaesser, Ultrafast spatiotemporal dynamics of terahertz generation by ionizing two-color femtosecond pulses in gases, Phys. Rev. Lett. 105, 053903 (2010). https://doi.org/10.1103/PhysRevLett.105.053903.

[69] J. Cook and R. M. Hochstrasser, Intense terahertz pulses by four-wave rectification in air, Opt. Lett. 25, 1210-1212 (2000). https://doi.org/10.1364/OL.25.001210.

[70] V. Vaičaitis, O. Balachninaitè, U. Morgner, and I. Babushkin, Terahertz radiation generation by three-color laser pulses in air filament, J. Appl. Phys. 125, 173103 (2019). https://doi.org/10.1063/1.5078683.

[71] J. D. Bagley, C. D. Moss, S. A. Sorenson, and J. A. Johnson, Laser-induced plasma generation of terahertz radiation using three incommensurate wavelengths, J. Phys. B: At., Mol. Opt. Phys. 51, 144004 (2018). https://doi.org/10.1088/1361-6455/aac6ef.

[72] P. B. Petersen, and A. Tokmakoff, Source for ultrafast continuum infrared and terahertz radiation, Opt. Lett. 35, 1962-1964 (2010). https://doi.org/10.1364/OL.35.001962.

[73] C. Lu, C. Zhang, L. Zhang, X. Wang, and S. Zhang, Modulation of terahertz-spectrum generation from an air plasma by tunable three-color laser pulses, Phys. Rev. A 96, 053402 (2017). https://doi.org/10.1103/PhysRevA.96.053402.

[74] P. G. Martinez, I. Babushkin, L. Berge, S. Skupin, E. Cabrera-Granado, C. Kohler, U. Morgner, A. Husakou, and J. Herrmann, Boosting terahertz generation in laser-field ionized gases using a sawtooth wave shape, Phys. Rev. Lett. 114, 183901 (2015). https://doi.org/10.1103/PhysRevLett.114.183901.

[75] J. Zhao, H. Gao, S. Li, C. Liu, Y. Chen, Y. Peng and Y. Zhu, Investigating the non-radially polarized component of terahertz wave emission during single-colour femtosecond laser filamentation in air, J. Opt. 20, 105502 (2018). https://doi.org/10.1088/2040-8986/aadef7.

[76] H.-C. Wu, J. Meyer-ter-Vehn, H. Ruhl, and Z.-M. Sheng, Terahertz radiation from a laser plasma filament, Phys. Rev. E 83, 036407 (2011). https://doi.org/10.1103/PhysRevE.83.036407.

[77] Y. Peng, T. Geng, X. Zang, L. Chen and Y. Zhu, Completely evolution of Gouy phase shift in longitudinal terahertz wave, 2016 41st Int. Conf. on Infrared, Millimeter, and Terahertz Waves (IRMMW-THz) (IEEE) pp. 1–2. https://doi.org/10.1109/IRMMW-THz.2016.7758846.

[78] I. Thiele, P. González de Alaiza Martínez, R. Nuter, A. Nguyen, L. Bergé, and S. Skupin, Broadband terahertz emission from two-color femtosecond-laser-induced microplasmas, Phys. Rev. A 96, 053814 (2017). https://doi.org/10.1103/PhysRevA.96.053814.

[79] M. Chen, A. Pukhov, X. Peng, and O. Willi, Theoretical analysis and simulations of strong terahertz radiation from the interaction of ultrashort laser pulses with gases, Phys. Rev. E 78, 046406 (2008). https://doi.org/10.1103/PhysRevE.78.046406.

[80] L. A. Johnson, J. P. Palastro, T. M. Antonsen, and K. Y. Kim, THz generation by optical Cherenkov emission from ionizing two-color laser pulses, Phys. Rev. A 88, 063804 (2013). https://doi.org/10.1103/PhysRevA.88.063804.

[81] V. A. Kostin and N. V. Vvedenskii, Ionization-induced conversion of ultrashort Bessel beam to terahertz pulse, Opt. Lett. 35, 247-249 (2010). https://doi.org/10.1364/OL.35.000247.

[82] A. V. Mitrofanov, D. A. Sidorov-Biryukov, M. M. Nazarov, A. A. Voronin, M. V. Rozhko, A. B. Fedotov, and A. M. Zheltikov, Coherently enhanced microwave pulses from midinfrared-driven laser plasmas, Opt. Lett. 46, 1081-1084 (2021). https://doi.org/10.1364/OL.410030.

[83] A. V. Mitrofanov, A. A. Voronin, M. V. Rozhko, D. A. Sidorov-Biryukov, M. M. Nazarov, A. B. Fedotov, and A. M. Zheltikov, Polarization and Spatial Mode Structure of Mid-Infrared-Driven Terahertz-to-Microwave Radiation, ACS Photon. 8, 1988 (2021). https://doi.org/10.1021/acsphotonics.0c01966.

Supplemental Materials

of

Traveling-wave antenna model for terahertz radiation from laser-plasma interactions

Jiayu Zhao,[1,2] Yuchen Hui,[1] Yamin Chen,[1] Zuanming Jin,[1] Alexander P. Shkurinov,[3] Yan Peng,[1,2,4] Yiming Zhu[1,2,*] and Songlin Zhuang[1]

[1] Terahertz Technology Innovation Research Institute, Shanghai Key Laboratory of Modern Optical Systems, School of Optical-Electrical and Computer Engineering, University of Shanghai for Science and Technology, Shanghai 200093, China.

[2] Shanghai Institute of Intelligent Science and Technology, Tongji University, Shanghai 200092, China.

[3] Faculty of Physics and International Laser Center, Lomonosov Moscow State University, Moscow 119991, Russia.

[4] py@usst.edu.cn

* ymzhu@usst.edu.cn

A. Derivation of the THz-plasma resonance effect

According to Fig. 1 of the main text, the process of plasma oscillation can be described as an electron being taken away from the equilibrium position in the post-ionization stage, which could be given by the classical Newton's second law:

$$m_e \frac{\partial \upsilon_e}{\partial t} = -eE - m\upsilon_e v_e + F_{laser} \tag{s1}$$

In Eq. (s1), m_e is the mass of an electron with the accelerated speed of $\partial \upsilon_e/\partial t$. eE represents the restoring force caused by the attraction from the stationary ion, where e denotes the electronic charge and E is the polarization electric field induced by the electron-ion separation. $m_e \upsilon_e v_e$ represents the damping force which is proportional to the momentum $m_e \upsilon_e$ and collision frequency v_e of electrons. F_{laser} represents the laser force derived from Ref. [s1]:

$$F_{laser} = \frac{e^2}{4c^2 m_e \varepsilon_0 (v_e^2 + \omega_0^2)} [\frac{\partial I}{\partial t} + 2v_e I] \tag{s2}$$

where ε_0 represents the vacuum permittivity, ω_0 is the laser frequency and I denotes the laser pulse intensity. F_{laser} mainly consists of the following two effects: the first one, involving the laser intensity gradient $\partial I/\partial t$, is associated with the ponderomotive force; and the second one is proportional to the collision frequency and corresponds to the radiation pressure.

Moreover, as for the conservation of electrons, there is $\partial N_e/\partial t + \partial N_e \upsilon_e/\partial z = 0$ in a unit volume as the well-known continuity equation, where N_e is the plasma density. Introducing integration to this equation and then taking $N_{e0} = \delta N_e + N_e$ and $\upsilon_e/c \rightarrow 0$ into account, it gives $\delta N_e = N_{e0} \upsilon_e/c$ (for $t = 0$, $\delta N_e = 0$ and $\upsilon_e = 0$). If the Gauss' law of $\text{div}D = e\delta N_e$ is further considered, $\upsilon_e = (\varepsilon_0 /eN_{e0}) \times \partial E/\partial t$ can be

deduced. This equation of υ_e and the plasma frequency $\omega_{pe} = (N_{e0} \, e^2/ \, m_e \varepsilon_0)^{1/2}$ as well as Eq. (s2) were substituted into Eq. (s1), which is now in form of

$$\frac{\partial^2 E}{\partial t^2} + \omega_{pe}^2 E + v_e \frac{\partial E}{\partial t} = \frac{e\omega_{pe}^2}{4c^2 m_e \varepsilon_0 (v_e^2 + \omega_0^2)}[\frac{\partial I}{\partial t} + 2v_e I] \tag{s3}$$

Via Fourier transform ($\partial/\partial t \sim -i\omega$), Eq. (s3) yields:

$$(-\omega^2 + \omega_{pe}^2 - iv_e \omega)E(\omega) = \frac{e\omega_{pe}^2}{4c^2 m_e \varepsilon_0 (v_e^2 + \omega_0^2)}[-i\omega + 2v_e]I(\omega) \tag{s4}$$

In view of the relationship of $j(\omega) = i\omega\varepsilon_0 E(\omega)$ between the displacement current and the polarization electric field, and assuming the laser pulse with duration of τ_L to be in the sine form of $I(\omega) = I_0 sin(\omega\tau_L/2)exp(-i\omega\tau_L/2)/\omega[(\omega\tau_L/2\pi)^2-1]$, the spectral current amplitude ($\omega_0 >> v_e$) can be written as

$$j(\omega) = \varepsilon_0 E_L \omega_{pe} \frac{\omega + 2iv_e}{2(\omega^2 - \omega_{pe}^2 + iv_e \omega)} \times \frac{\sin(\omega\tau_L / 2)}{1 - (\omega\tau_L / 2\pi)^2} e^{-i\omega\tau_L/2} \tag{s5}$$

where $E_L = e\omega_{pe}I_0/2m_e\varepsilon_0 c^2 \omega_0^2$ is the amplitude of the plasma wave driven by the laser ponderomotive force. And the radiated spectrum given by $E_{rad}(\omega) \propto i\omega j(\omega)$ [s2] is

$$E_{rad}(\omega) \propto i\omega \, \varepsilon_0 E_L \omega_{pe} \frac{\omega + 2iv_e}{2(\omega^2 - \omega_{pe}^2 + iv_e \omega)} \times \frac{\sin(\omega\tau_L / 2)}{1 - (\omega\tau_L / 2\pi)^2} e^{-i\omega\tau_L/2} \tag{s6}$$

which is also shown in the main text as Eq. (3).

B. The effect of the longitudinal DC electric field on the plasma current

When the plasma filament is applied with a external DC field (E_{ex}^l) along the longitudinal axis, Eq. (s1) can be transformed into the following Eq. (s7):

$$m_e \frac{\partial \upsilon_e^l}{\partial t} = -eE_p^l - eE_{ex}^l - m_e \upsilon_e^l v_e + F_{laser} \tag{s7}$$

Via Fourier transformation, the electron velocity in the longitudinal direction is written as $v_e^l = [e(E_p^l + E_{ex}^l) - F_{laser}]/m_e(i\omega - v_e)$, which is further accelerated by the additional E_{ex}^l. In this case, the spectral current can be deduced by similar derivation processes as Eq. (s1-s5), and the result is

$$j(\omega) = \varepsilon_0 E_L \omega_{pe} \frac{\omega + 2iv_e}{2(\omega^2 - \omega_{pe}^2 + iv_e \omega)} \times \frac{\sin(\omega\tau_L / 2)}{[1 - (\omega\tau_L / 2\pi)^2]} e^{-i\omega\tau_L/2} + \frac{\varepsilon_0 E_{ex}^l \omega_{pe}^2}{\omega^2 - \omega_{pe}^2 + iv_e \omega} \tag{s8}$$

Consequently, the spectral current amplitude is the sum of two terms, i.e., $j = j_w + j_{ex}^l$, where the first one is the wake current spectrum as shown in Eq. (s5), and the second spectral current is excited by the external electric field:

$$j_{ex}^l(\omega) = \frac{\varepsilon_0 E_{ex}^l \omega_{pe}^2}{\omega^2 - \omega_{pe}^2 + i\nu_e\omega} \tag{s9}$$

For comparison between j_w and j_{ex}^l, calculations of Eq. (s5) and (s9) have been carried out, and the results are shown in Fig. (s1). It can be seen that with E_{ex}^l of 1 kV/cm (green dot and dash line), the additional current j_{ex}^l is already comparable with the original j_w (black line) whose laser wakefield amplitude $E_w \left(= E_L 2\nu_e\tau_L\omega/\omega_{pe}\right)$ is reported in the order of magnitude of several hundred V/cm (e.g., 0.2 kV/cm in Ref. [s3]). With a larger E_{ex}^l of 5 or 10 kV/cm as used in Ref. [s4], the spectral currents can be further increased significantly as expected. In this case, j_{ex}^l in Eq. (s9) dominates the THz wave generation, and the direction of E_{ex}^l (i.e., $\pm E_{ex}^l$) won't change the radiated THz intensity since j_w is neglectable [s4].
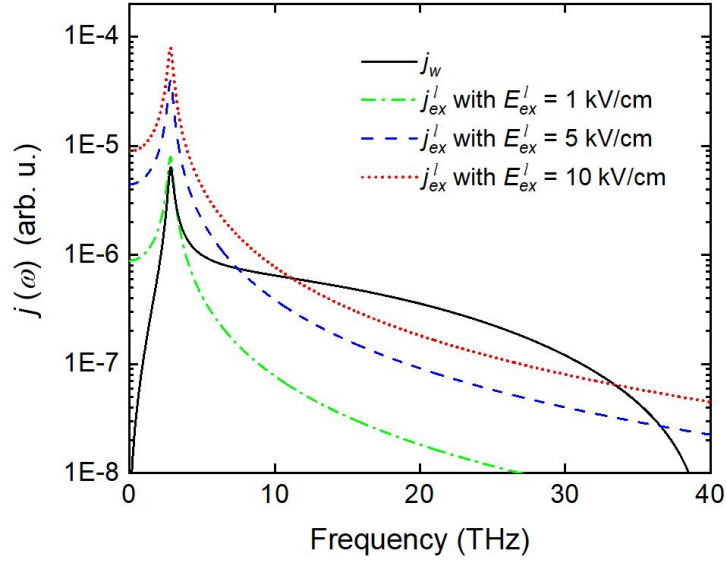
Fig. s1 The wake current spectrum (black line) and the additional spectral currents with longitudinal external electric fields of 1 kV/cm (green dot and dash line), 5 kV/cm (blue dashed line) and 10 kV/cm (red dotted line), respectively.

Therefore, we come to the conclusion that the electric current driven by the external field could greatly exceed the current induced by the ponderomotive force, as long as the employed DC value reaches the level of kV/cm. At the same time, not only the plasma current, but also the THz energy is much enhanced during filamentation. In consideration of the above analyses with our microscopic model, we accordingly detailed the definition of the gain coefficient n as $n = 1 + |E_{ex}^l/E_w|$ in our macroscopic (TWA) model as shown in Table I of the main text.

Revisiting Fig. s1, towards low frequencies such as 0.1 THz, the spectral current j_{ex} (green dot and dash line) excited by the external electric field E_{ex} is about two orders of magnitude larger than the original j_w (black line) given by the laser wakefield. For this reason, j_w was not included in our calculations at 0.1 THz (Table I), and the THz yield is solely proportional to $|j_{ex}|$ (also $|E_{ex}|$, see Eq. s9). Thus we stated

that the direction of E_{ex} (i.e., $\pm E_{ex}$) won't change the radiated THz intensity. However, if larger THz frequency (>0.1 THz) is considered, one can also see in Fig. s1 that, j_w rapidly increased and even exceeded j_{ex} at around 2 THz. This time, j_w is no longer negligible and the total THz yield is decided by Eq. s8 as [$j_w + j_{ex}(E_{ex})$], which is now influenced by the sign of E_{ex}. From Eq. s8, we can further predicted that the minimum THz yield is obtained at a negative E_{ex} (= $-j_w/j_{ex}$), thus in agreement with Fig. 2(a) of [Phys. Rev. E 102, 063211 (2020)].

C. The effect of the transverse DC electric field on the plasma current

As for the presence of a transverse DC field E_{ex}^t, Eq. (s1) is re-considered in the transverse direction and can be changed into

$$m_e \frac{\partial \upsilon_e^t}{\partial t} = -eE_p^t + eE_{ex}^t - m_e \upsilon_e^t v_e \qquad (s10)$$

In the same way as Eq. (s1-s5), the transverse spectral current amplitude can be obtained:

$$j_{ex}^t(\omega) = -\frac{\varepsilon_0 E_{ex}^t \omega_{pe}^2}{\omega^2 - \omega_{pe}^2 + iv_e\omega} \qquad (s11)$$

which has the similar expression with that induced by the longitudinally external field as shown in Eq. (s9), and the effect of j_{ex}^t will also be noticeable when E_{ex}^t is close to (or larger than) E_w.

In this condition, the combination of the transverse current j_{ex}^t and the original longitudinal current j_w (Eq. (s5)) determines the total THz yield, for which reason $\varphi = \arctan(E_{ex}^t/E_w)$ is defined to describe the angle between the direction of the current element and the filament axis in the TWA model as shown in Table I of the main text.

D. Estimate of the THz conversion efficiency

Here we calculated the THz power conversion efficiency given by the resonance radiation theory. Based on the proportional relationship shown in Eq. (s6), it is now transformed into Eq. (s12) by being multiplied with a factor of $A/4\pi\varepsilon_0 c^2$ [s5], where A is the area of the current cross section, roughly in diameter of 100 μm in case of a plasma filament.

$$E_{rad}(\omega) = \frac{A}{4\pi\varepsilon_0 c^2} \times i\omega\, \varepsilon_0 E_L \omega_{pe} \frac{\omega + 2iv_e}{2(\omega^2 - \omega_{pe}^2 + iv_e\omega)} \times \frac{\sin(\omega\tau_L/2)}{1 - (\omega\tau_L/2\pi)^2} e^{-i\omega\tau_L/2} \qquad (s12)$$

Then, the power spectral density of the generated THz wave can be described as

$$\frac{dW_{rad}(\omega)}{d\omega} = \frac{\left|E_{rad}(\omega)\right|^2}{2\eta} S \qquad (s13)$$

where $\eta = 377\ \Omega$ is the optical impedance, and S is the area of THz radiation spot, normally within a diameter of millimeter scale (set 2 mm as an example). At last, the generated THz power can be obtained by spectral integral of Eq. (s13) in the range from 0 to 200 THz, and the result is about 1.26×10^{-10} W. Reminding ourselves that the input laser power in our case is ~1 W, thus the conversion efficiency is of the order of magnitude of ~10^{-10}. This value is slightly larger than the reported 10^{-11} [s3] for the transition-Cherenkov mechanism, but still much lower than that of the two-color laser pumping scheme (~10^{-4}).

E. Calculation of the electron collision frequency

For laser plasma in ambient air pressure similar with our situation, the mean free time of electron collision (or the scattering time) is constantly reported on the order of hundreds of femtoseconds [s6-s11], corresponding to the electron collision frequency in terahertz scale (mostly 1-5 THz) [s1, s3, s4, s12-s14], based on which 2 THz was adopted in the main text (Section 3.1).

We have also revisited the value of electron collision frequency with formulas widely accepted in literature in the community [s1, s13-s18]. The electron collision frequency (v_e) being considered during THz wave radiation is given by

$$v_e = v_{en} + v_{ei} \tag{s14}$$

where v_{en} and v_{ei} are the electron-neutral and electron-ion collision frequencies, respectively. Here, v_{en} can be computed by

$$v_{en} = N_n \sigma_0 \left(k_B T_e / m_e \right)^{1/2} \tag{s15}$$

where $N_n = N_{n0} - N_e$ is the neutral density with the ambient $N_{n0} = 2.7\times10^{19}$ cm^{-3}, k_B is the Boltzmann constant, and $\sigma_0 \sim 10^{-15}$ cm^2 [s19-s21] is a typical value for the scattering cross section. In practical units, v_{en} can be simplified as v_{en}[Hz]$= 4\times10^{-8} N_n$[cm^{-3}]T_e[eV]$^{1/2}$. And v_{ei} is given by

$$v_{ei} = \frac{\sqrt{2}}{3\sqrt{\pi}} N_e \left(\frac{Ze^2}{4\pi\varepsilon_0} \right)^2 \frac{4\pi}{m_e^{1/2} T_e^{3/2}} \ln\Lambda \tag{s16}$$

which can also be written simply as v_{ei}[Hz]$= 3\times10^{-6}$ (lnΛ)N_e[cm^{-3}]/T_e[eV]$^{3/2}$. For the parameters of our experiment, with lnΛ=5, N_e=10^{17} cm^{-3} and T_e = 1 eV at 300K, v_e is calculated as v_e = 1.05 (v_{en}) + 1.45 (v_{ei}) = 2.5 THz, which is close to the value used in the main text.

F. Discussions about the plasma-THz resonance phenomenon

As put in Ref. [s22], strong resonant enhancement of the THz radiation was observed if the plasma frequency ($\omega_p/2\pi$) was close to the inverse pulse length of the pumping laser (t_0 = 120~140 fs, thus $1/t_0$ is in THz band). Furthermore, this work indicates that (i) the frequency of THz emission varied with the gas density (by changing the ambient gas pressure) and was close to the bulk plasma

frequency as shown in its Fig. 3, and (ii) the THz signal was attributed to the nonlinear current in its Eq. (1), whose denominator contained the item of $[1-(\omega_p/\omega)^2]$. Both (i) and (ii) reveal that maximum THz signals could be achieved at $\omega_p=\omega_{THz}$.

Although the concept of plasma-THz resonance was not directly raised in Ref. [s22], the above relationships showed the clue. However, here we want to emphasize solely on the phenomenal similarities between Ref. [s22] and our work (Section 3 of the main text, e.g., Fig. 2b$_1$), while the underlying mechanisms might be very different because of the used relativistic laser pulses for generating THz radiation in Ref. [s22]. Accordingly. the resulting experimental configurations, like the focused laser intensity or the plasma density, could be much larger than the laser equipment used by us, leading to more complicated physics.

It can also be noticed that Ref. [s22] is often cited as the first demonstration of single-color laser-ionization induced THz wave generation in the community, but the following works were mostly carried out with non-relativistic lasers. In the non-relativistic case, we base on the quasi-Cherenkov model (Ref. [6] of the main text) and understand the THz radiation better with the concept of travelling-wave antenna in certain aspects, as we put in the Introduction of the main text. On the other hand, the plasma filament has been studied in quite a different way in this work. For us, the THz resonant radiation was mainly investigated by its longitudinal evolution along the filament (Fig. 3-5 of the main text), rather than collecting the signal from the whole filament. This is a new view in our field to the best of our knowledge.

Reference

[s1] P. Sprangle, J. R. Penano, B. Hafizi, and C. A. Kapetanakos, Ultrashort laser pulses and electromagnetic pulse generation in air and on dielectric surfaces, Phys. Rev. E 69, 066415 (2004). https://doi.org/10.1103/PhysRevE.69.066415.

[s2] K. Y. Kim, A. J. Taylor, J. H. Glownia, and G. Rodriguez, Coherent control of terahertz supercontinuum generation in ultrafast laser–gas interactions, Nat. Photonics 2, 605-609 (2008). https://doi.org/10.1038/nphoton.2008.153.

[s3] C. D'Amico, A. Houard, S. Akturk, Y. Liu, J. Le Bloas, M. Franco, B. Prade, A. Couairon, V. T. Tikhonchuk, and A. Mysyrowicz, Forward THz radiation emission by femtosecond filamentation in gases: theory and experiment, New J. Phys. 10, 013015 (2008). https://doi.org/10.1088/1367-2630/10/1/013015.

[s4] Y. Liu, A. Houard, B. Prade, A. Mysyrowicz, A. Diaw, and V. T. Tikhonchuk, Amplification of transition-Cherenkov terahertz radiation of femtosecond filament in air, Appl. Phys. Lett. 93, 051108 (2008). https://doi.org/10.1063/1.2965612.

[s5] J. Xu, and X. C. Zhang, Terahertz science technology and applications [M], Beijing: Peking University Press, 2007, ISBN:9787301125038.

[s6] M. Kreß, T. Löffler, M. D. Thomson, R. Dörner, H. Gimpel, K. Zrost, T. Ergler, R. Moshammer, U. Morgner, J. Ullrich, and H. G. Roskos, Determination of the carrier-envelope phase of few-cycle laser pulses with terahertz-emission spectroscopy, Nat. Phys. 2, 327–331(2006). https://doi.org/10.1038/nphys286.

[s7] K. Y. Kim, J. H. Glownia, A. J. Taylor, and G. Rodriguez, Terahertz emission from ultrafast ionizing air in symmetry-broken laser fields, Opt. Express 15, 4577-4584 (2007). https://doi.org/10.1364/OE.15.004577.

[s8] H. G. Roskos, M. D. Thomson, M. Kreß, and T. Löffler, Broadband THz emission from gas plasmas induced by femtosecond optical pulses: From fundamentals to applications, Laser & Photon. Rev. 1, 349-368 (2007). https://doi.org/10.1002/lpor.200710025.

[s9] G. Rodriguez, C. W. Siders, C. L. Guo, and A. J. Taylor, Coherent ultrafast MI-FROG spectroscopy of optical field ionization in molecular H_2, N_2, and O_2, IEEE J. Sel. Top. Quantum Electron 7(4), 579 (2001). https://doi.org/10.1109/2944.974229.

[s10]A. Couairon and A. Mysyrowicz, Femtosecond filamentation in transparent media, Phys. Rep. 441, 47–189 (2007). https://doi.org/10.1016/j.physrep.2006.12.005.

[s11]W. Liu, Intensity Clamping During Femtosecond Laser Filamentation, Chin. J. Phys. 52, 1-II:465-489 (2014). http://dx.doi.org/10.6122/CJP.52.465.

[s12]C. D'Amico, A. Houard, M. Franco, B. Prade, A. Mysyrowicz, A. Couairon, and V. T. Tikhonchuk, Conical forward THz emission from femtosecond-laser-beam filamentation in air, Phys. Rev. Lett. 98, 235002 (2007). https://doi.org/10.1103/PhysRevLett.98.235002.

[s13]M. Alshershby, Z. Hao, and J. Lin, Guiding microwave radiation using laser-induced filaments: the hollow conducting waveguide concept, J. Phys. D: Appl. Phys. 45, 265401 (2012). https://doi.org/10.1088/0022-3727/45/26/265401.

[s14]R. R. Musin, M. N. Shneider, A. M. Zheltikov, and R. B. Miles, Guiding radar signals by arrays of laser-induced filaments: finite-difference analysis, Appl. Opt. 46, 5593-5597 (2007). https://doi.org/10.1364/AO.46.005593.

[s15]https://ocw.mit.edu/courses/nuclear-engineering/22-611j-introduction-to-plasma-physics-i-fall-2006/readings/

[s16]V.L. Ginzburg, W.L. Sadowski, D.M. Gallik, and S.C. Brown, Propagation of Electromagnetic Waves in Plasma, London: Gordon and Breach, 1997.

[s17]J. D. Huba, Plasma Formulary, Naval Research Laboratory Publication NRL/PU/6790-98-358 U.S. GPO, Washington, D.C. 1998.

[s18]https://en.wikipedia.org/wiki/Plasma_parameters

[s19]V.P. Kandidov, O.G. Kosareva, I.S. Golubtsov, W. Liu, A. Becker, N. Akozbek, C.M. Bowden, and S.L. Chin, Self-transformation of a powerful femtosecond laser pulse into a white-light laser pulse in bulk optical media (or supercontinuum generation), Appl. Phys. B 77, 149–165 (2003). https://doi.org/10.1007/s00340-003-1214-7.

[s20]S.L. Chin, S.A. Hosseini, W. Liu, Q. Luo, F. Théberge, A. Becker, N. Akozbek, V.P. Kandidov, O.G. Kosareva, and H. Schroeder, The propagation of powerful femtosecond laser pulses in opticalmedia: physics, applications, and new challenges, Can. J. Phys. 83, 9 (2005). https://doi.org/10.1139/p05-048.

[s21]Yu.P. Raizer, Gas discharge physics, Springer-Verlag, New York. 1991. ISBN:3540194622.

[s22]H. Hamster, A. Sullivan, S. Gordon, W. White, and R. W. Falcone, Subpicosecond, electromagnetic pulses from intense laser-plasma interaction, Phys. Rev. Lett. 71, 2725-2728 (1993). https://doi.org/10.1103/PhysRevLett.71.2725.